CARDIFF UNIVERSITY
PRIFYSGOL CAERDYDD

ORCA – Online Research @ Cardiff

This is an Open Access document downloaded from ORCA, Cardiff University's institutional repository:https://orca.cardiff.ac.uk/id/eprint/73216/

This is the author's version of a work that was submitted to / accepted for publication.

Citation for final published version:

Alnaas, W. F. and Jefferson, A. D. 2016. A smooth unloading-reloading approach for the nonlinear finite element analysis of quasi-brittle materials. Engineering Fracture Mechanics 152 , pp. 105-125. 10.1016/j.engfracmech.2015.04.018

Publishers page: http://dx.doi.org/10.1016/j.engfracmech.2015.04.01...

Please note:
Changes made as a result of publishing processes such as copy-editing, formatting and page numbers may not be reflected in this version. For the definitive version of this publication, please refer to the published source. You are advised to consult the publisher's version if you wish to cite this paper.

This version is being made available in accordance with publisher policies. See http://orca.cf.ac.uk/policies.html for usage policies. Copyright and moral rights for publications made available in ORCA are retained by the copyright holders.

A smooth unloading-reloading approach for the nonlinear finite element analysis of quasi-brittle materials

W F Alnaas & A D Jefferson

ABSTRACT

This paper presents a new method for improving the robustness and convergence characteristics of a finite element damage model for quasi-brittle materials. In this method, a smooth unloading-reloading function (SUR) is employed to compute an approximate tangent matrix in a Newton type solution procedure. A new method is also presented for predicting a converged value of the damage parameter. The performance of the new methods are assessed using a range of idealised quasi-brittle specimens. Results show that the new SUR approaches are robust and result in considerable savings relative to solutions obtained with a secant unloading-reloading function.

Keywords: *Damage, constitutive model, non-linear finite element analysis, quasi-brittle materials.*

Email: AlnaasWF1@cardiff.ac.uk

Tel: +4407809282471

Fax: +44 (0)29 2087 4939

Nomenclature

a_k	Constant used in computing Softening curve constants
a_p	Softening function constant
a_t	Softening function constant
c_1	Softening function constant
$\mathbf{D_0}$	Elastic stiffness matrix
$\mathbf{D}_{tan}$	Constitutive tangent matrix
E	Young's modulus
$\mathrm{E_c}$	Young's modulus of concrete
$\mathrm{E_s}$	Young's modulus of steel
f_s	Target softening function
f_t	Tensile strength
G_f	Fracture energy
It	Iteration number
m	Softening function constant
r_0	Effective end of the softening curve
r_{eff}	Effective damage evolution parameter
r_k	Damage evolution parameter at the peak of the uniaxial stress curve
r_p	Damage evolution parameter
r_{pp}	Predictive damage evolution parameter
r_t	Effective damage strength parameter= $f_t/\sqrt{E}$
r_ε	Limiting damage evolution parameter ratio
β	Softening curve constant
Δr_p	Iterative change in damage evolution parameter
$\boldsymbol{\varepsilon}$	Strain tensor
ε_0	Strain at the effective end of softening curve
ε_t	Tensile strain measure
η	Target softening curve constant
η_k	Normalised damage evolution parameter
ν	Target softening curve constant
υ	Poisson's ratio
$\boldsymbol{\sigma}$	Stress tensor
$\boldsymbol{\sigma_0}$	Effective stress
σ_k	Stress to which the SUR function is asymptotic
σ_p	Smooth unloading-loading function
Ψ_d	Tolerance value for displacement norm
Ψ_f	Tolerance value for out of balance force norm
ω	Basic damage variable ($\omega \in [0,1]$)
ω_p	SUR damage parameter

ω_{pf}	Damage parameter controlling linear part of the SUR function

1. Introduction

Micro-cracking is a feature of quasi-brittle (QB) materials loaded beyond their elastic limit and is the primary cause of stiffness and strength degradation in materials such as concrete and rock. Laboratory samples of quasi-brittle material frequently exhibit a post-peak softening response when loaded in tension or unconfined compression. This macro-scopic softening behaviour is sometimes referred to as material softening although it is recognised that this is a structural phenomenon, resulting from the micro-cracking, rather than a fundamental response of the material [1-4].

Softening behaviour has presented researchers with two related computational challenges; namely, how to (i) obtain mesh-objective predictions and (ii) find minimum energy converged solutions in an efficient manner. Mathematically, these issues are a consequence of the loss of ellipticity of the governing partial differential equations [5] , when a certain degree of damage is exceeded, and are characterised by the associated stiffness matrix becoming non-positive definite.

The first of the above challenges can be dealt with, at least to first order accuracy, by using the crack-band model of Bažant and Oh [6]. More refined means of resolving the mesh-sensitivity problems include the use of integral [7, 8] and differential [9-12] non-local models. However, resolving the mesh sensitivity issue does not resolve of all the stability and convergence issues associated with modelling QB materials.

The nonlinear equations resulting from the finite element simulation of QB structures are frequently solved using incremental-iterative solution schemes based on Newton-Raphson (NR) algorithms [5, 13]. It is the poor convergence properties of these solution schemes, when solving problems involving QB materials, which so frequently cause frustration to finite element analysts. It is this issue that provides the motivation for the work of this paper.

Many approaches have been made to improve the efficiency of these NR procedures and to improve their robustness [5, 13-17]. These techniques include replacing standard Newton schemes with Quasi-Newton approaches[13, 14, 17] and accelerated NR methods, amongst which line-search algorithms are one of the most effective techniques [5, 13, 15, 16].

When the global response of a structure softens and exhibits ‘snap-back’ behaviour, arc-length procedures can allow the complete equilibrium path to be traced [5, 13, 17-21]. The constraints provided by the arc-length methods can also help to improve the overall stability of a solution as

well as allowing solutions to be obtained when local snap-backs occur. Another approach for tracing global snap-back is Ladevese's LATIN method [22], which has undergone significant development in recent years [23, 24].

None of the aforementioned algorithms are completely robust, nor do they fully resolve all the stability and convergence difficulties encountered when analysing QB structures. These on-going difficulties have undoubtedly been behind the development of solution algorithms that avoid multiple iterations. These methods include the 'implicit-explicit' approach of Oliver et al [25, 26], in which a projected state variable (e.g. a damage parameter) is used to determine a predicted consistent tangent matrix that is exact for the current increment but for which a correction is made in the subsequent stress-recovery phase. An alternative non-iterative method, called the 'Sequentially Linear Approach (SLA)', was proposed by Rots [27]. This method uses a 'saw-tooth' function to replace the post-peak softening function. Rots and Invernizzi [28] and Rots et al [29] later improved the SLA to achieve mesh independent behaviour. The SLA has also been extended to allow the simulation of non-proportional loading [30, 31], as well as being applied to the analysis of concrete beams which fail in shear [32].

The numerical robustness of implicit-explicit and SLA approaches cannot be questioned and their effectiveness at dealing with a certain class of problem has been demonstrated. Despite the fact that there are considerable benefits to using these approaches, they can result in non-smooth responses, and would require further development before being able to cope well with constitutive models that include non-linear crack closure in combined shear and normal modes. Currently they are not compatible with non-linear plasticity models for other materials, which would be an issue for solving soil-structure problems.

In seeking an alternative to the above approaches, we explored the convergence properties of an isotropic damage model, with a number of different unloading-reloading functions, when applied to the finite element analysis of a range of idealised QB fracture problems. In each case, the reference solution was obtained using a model with secant unloading-reloading behaviour. This study showed that enormous savings in computational time, with respect to this reference solution, are achievable by using a smooth nonlinear unloading-reloading function. The study led in turn to the development of a new algorithm for predicting damage states and thereby further accelerating solutions. The new method, named the Smooth Unloading-Reloading (SUR) approach, is described in this paper along with the new predictive algorithm. The remainder of this paper is arranged as follows:

Section 2 provides a description of the isotropic damage model used for the study;

Section 3 presents the SUR and the target softening functions;

Section 4 gives a new expression for predicting the converged value of a damage evolution parameter;

Section 5 presents results from the analysis of a range of idealised fracture problems, to illustrate the performance and convergence characteristics of the SUR and predictive SUR approaches;

Section 6 draws a number of conclusions from the study.

2. Constitutive model

In the present study, the SUR algorithm is employed with an isotropic damage model [33, 34]. This is based on the simplifying assumption that stiffness degradation is isotropic and the loss of material stiffness is characterised by a scalar damage variable ($\omega \in [0, 1]$). The constitutive equation for the isotropic damage model is expressed as:

$$\boldsymbol{\sigma} = (\boldsymbol{I} - \omega)\, \mathbf{D}_0 : \boldsymbol{\varepsilon} \tag{1}$$

where $\boldsymbol{\sigma}$ and $\boldsymbol{\varepsilon}$ are the stress and strain tensors respectively; $\mathbf{D}_0$ donates the elastic stiffness of the undamaged material and the damage variable ω is a function of a damage evolution parameter r_p.

The standard form of the constitutive equations for the isotropic damage model are summarised in Box 1, in which the effective stress $\boldsymbol{\sigma}_0 = \mathbf{D}_0 : \boldsymbol{\varepsilon}$:

Box 1: Summary of isotropic damage model algorithm [25, 33-35]	
$\boldsymbol{\sigma} = (1-\omega)\, \mathbf{D}_0 : \boldsymbol{\varepsilon}$	Constitutive equation
$r_p = r_{eff} \quad r_p \mid_{t=0} = r_k \quad r_p \geq r_k$ $r_{eff} = \sqrt{\boldsymbol{\sigma}_0^{+} : \mathbf{D}_0^{-1} : \boldsymbol{\sigma}_0^{+}}$	Damage evolution parameter
$f(r_{eff}, r_p) = r_{eff} - r_p$	Damage function
$\dot{r}_p \geq 0; \quad f \leq 0; \quad \dot{r}_p f = 0;$	Damage function loading/unloading Conditions

$\mathbf{D}_{tan} = \begin{cases} (1-\omega)\mathbf{D_0} & \forall\, r_{eff} < r_p \\ (1-\omega)\mathbf{D_0} - \dfrac{d\omega}{dr_p}\boldsymbol{\sigma}_{\mathbf{0}} : \left(\mathbf{D_0} \otimes \dfrac{dr_p}{d\boldsymbol{\sigma}}\right)^T & \forall\, r_{eff} \geq r_p \end{cases}$	Constitutive tangent operator

where r_{eff} is a scalar measure of the current 'effective' stress, $\boldsymbol{\sigma}_{\mathbf{0}}^{+}$ denotes the positive part of the effective stress tensor, which is defined as:

$$\boldsymbol{\sigma}_{\mathbf{0}}^{+} = \sum_{i=1}^{3} \left\langle \boldsymbol{\sigma}_{\mathbf{0}i} \right\rangle \mathbf{p}_i \otimes \mathbf{p}_i \tag{2}$$

where $\left\langle \boldsymbol{\sigma}_{\mathbf{0}i} \right\rangle$ stands for the positive part of the *i*th principal effective stress $\boldsymbol{\sigma}_{\mathbf{0}i}$, $\mathbf{p}_i$ represents the *i*th stress eigenvector. Symbol $\otimes$ denotes the tensor product, and symbol $\langle \mathbf{x} \rangle$ is the Macaulay bracket.

Physically, r_p is a scalar measure of the largest effective stress ever reached in the history of the material up to the current state. The damage function $f(r_{eff}, r_p)$ is defined in terms of effective stress space. The tangent constitutive operator $\mathbf{D}_{tan}$ changes for unloading ($\forall\ r_{eff} < r_p$) and reloading ($\forall\ r_{eff} \geq r_p$) processes.

In the standard form of the model, the damage parameter (ω) depends directly upon a softening function $f_{ss}(r_p)$ according to the following relationship;

$$\omega(r_p) = 1 - \frac{f_{ss}(r_p)}{r_p} \tag{3}$$

A standard exponential form for this softening function is as follows;

$$f_{ss}(r_p) = \begin{cases} f_t & \forall \quad r_{eff} \leq r_t \\ f_t e^{-c1\frac{(r_{eff} - r_t)}{(r_0 - r_t)}} & \forall \quad r_{eff} > r_t \end{cases} \tag{4}$$

in which f_t is the tensile strength, E is Young's modulus, c_1=5, $\varepsilon_t = f_t/\mathrm{E}$, $r_t = \varepsilon_t \cdot \sqrt{\mathrm{E}}$, $r_0 = \varepsilon_0 \cdot \sqrt{\mathrm{E}}$ and ε_0 is the strain at the effective end of the softening curve.

It should be noted that the above form of f_{ss} is introduced only to provide a complete description of the standard model. This softening function is not used in the new model but is replaced by the target function f_s given in the next section of this paper.

To avoid mesh dependent behaviour, ε_0 is computed from the fracture energy parameter G_f and the element characteristic length l_{ch} using Bazant and Oh's crack-band approach [6]. The characteristic length is directionally dependent within an element and is calculated to be equal to the length of the longest straight line that could be drawn within a finite element in the direction of the major principal strain axis.

3. Smooth unloading-reloading and target damage evolution functions

The proposed SUR approach uses a target function $f_s(r_p)$ and a smooth unloading-reloading function $\sigma_p(r_p, r_{eff})$, as illustrated in figure 1. It may be seen that the SUR function has two parts; (**i**) when $r_{eff} < a_p r_p$, for which linear unloading-reloading with a slope $(1-\omega_{pf})\mathrm{E}$ is assumed, and (**ii**) when $r_{eff} \geq a_p r_p$, for which nonlinear unloading-reloading is a assumed, according to the function $\sigma_p(r_p, r_{eff})$.

The SUR function depends on the damage evolution parameter (r_p), which is updated for every iteration within each load/displacement increment from the value obtained at the last converged increment.

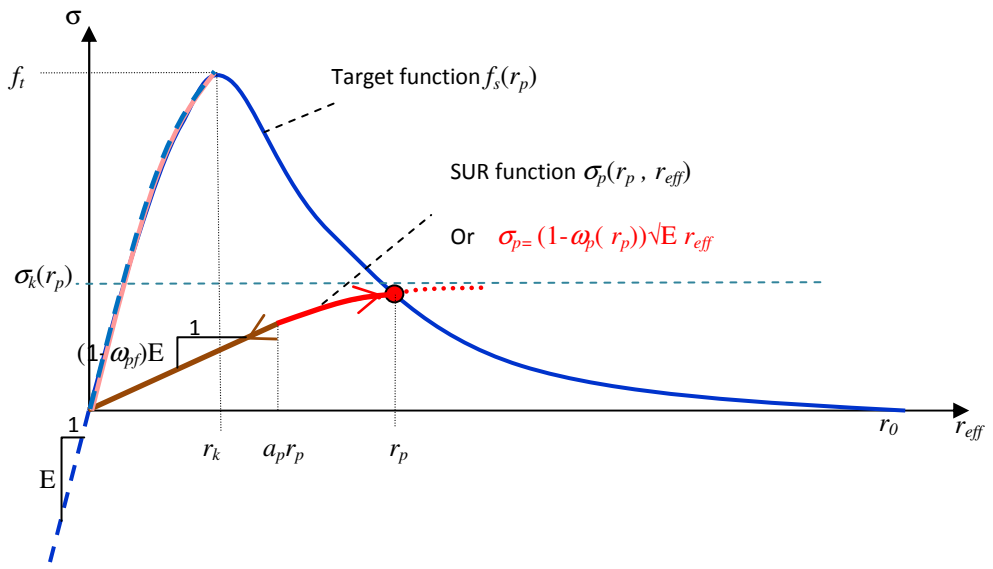

Figure 1. Target and unloading-reloading damage evolution functions.

It should be noted that the unloading-reloading response shown in figure 1 more accurately represents the response measured in tests than does a function based on secant unloading-reloading [36]. The true unloading-reloading response exhibits hysteresis behaviour that is not simulated here. Rather, the model employs a function that closely represents the real reloading curve. The authors acknowledge that this is a simplification but consider these hysteresis effects to be second-order in the simulation of most plain and reinforced concrete structures.

The target function gives the equivalent uniaxial stress and depends on the damage evolution parameter r_p, which in 1D, is directly proportional to the maximum strain experienced. The complete uniaxial curve, upon which the target curve is based, is given in equation (5).

$$f_s(r_p) = \begin{cases} \sqrt{\mathrm{E}} \cdot r_p & \forall \quad r_p < r_{t0} \\ \dfrac{a_t \cdot f_t}{\beta - 1} \cdot e^{-c_1 \cdot \eta} \cdot (\beta - e^{-c_1 \cdot m \cdot \eta}) & \forall \quad r_p \geq r_{t0} \end{cases} \tag{5}$$

where $r_t = \varepsilon_t \cdot \sqrt{\mathrm{E}}$, $r_{t0} = r_t \cdot a_t$, , $r_\varepsilon = r_0 / r_t$ and $r_k = r_t \cdot a_k$. ε_0 is the strain at the effective end of the of the target softening curve; $\eta = \dfrac{r_p - r_{t0}}{r_0 - r_{t0}}$; $\eta_k = \dfrac{a_k - a_t}{r_\varepsilon}$.

The expressions used to compute m, β, and a_t, along with their derivations, are given in Appendix A. Parameter a_k follows from the form of the SUR function and is given after equation (7). This means that m, β, a_t, and a_k are all dependent parameters, governed by the function's boundary conditions (see Appendix A) and the form of the SUR function and its associated parameters. Whilst the pre-peak and post-peak parts of the target function are given in equation (5) for completeness, the proposed algorithm only employs f_s from the peak onwards, as explained later in this section.

The SUR function is tangential to the secant curve with modulus $[(1\text{-}\omega_{pf})\mathrm{E}]$, and is asymptotic to the stress $\sigma_k(r_p)$ in equation (7) and takes the form as:

$$\sigma_p(r_p, r_{eff}) = \sigma_k(r_p) \cdot \left[1 - (1 - \frac{a_p}{v}) \cdot e^{-\left[\frac{r_{eff} - a_p r_p}{(v - a_p) r_p} \right]} \right] \tag{6}$$

in which the constants v and a_p, take default values of 0.70 and 0.75 respectively, although the effect on the numerical performance of the model of varying these parameters is explored in section 5.5. These default values provide a reasonable representation of the reloading response measured in cyclic uniaxial fracture tests [36] and the values can be directly calibrated using data from such tests.

However, it is emphasised that the aim of the present work is directed towards improving the stability and robustness of solutions to fracture problems and not towards improving the accuracy of existing damage models. The value of the damage evolution parameter at the peak of the uniaxial stress curve is denoted r_k. The initial value of r_p is set to r_k (i.e. the value at the peak of the target softening function).

σ_p depends upon the asymptotic stress function σ_k, which is defined as follows;

$$\sigma_k(r_p)=\begin{cases} f_s(r_k)\cdot v\cdot a_k & \forall \quad r_p \le r_k \\ f_s(r_p)\cdot v\cdot a_k & \forall \quad r_p > r_k \end{cases} \tag{7}$$

noting that $f_s(r_k)=f_t$

The above expressions for σ_k are obtained by equating σ_p from equation (6) to f_s from equation (5), for a given value of r_p i.e. the curve coincides at $r_{eff} = r_p$.

Using equation (7) in (6) and again considering the condition $f_s(r_p)=\sigma_p$ *at* $r_{eff}=r_p$, leads to the following expression for a_k;

$$a_k = \frac{1}{v\cdot\left[1-(1-\frac{a_p}{v})\cdot e^{-\left[\frac{1-a_p}{v-a_p}\right]}\right]}$$

The damage parameter that controls the linear part of the SUR function is computed as:

$$\omega_{pf}(r_p)=\begin{cases} 0 & \forall \quad r_p \le r_k \\ 1-\dfrac{\sigma_k}{v\cdot r_p\cdot\sqrt{\mathrm{E}}} & \forall \quad r_p > r_k \end{cases} \tag{8}$$

and the damage parameter for the SUR function is given by:

$$\omega_p(r_p,r_{eff})=\begin{cases} \omega_{pf} & \forall \quad r_{eff} \le a_p r_p \\ 1-\dfrac{\sigma_p(r_p,r_{eff})}{\sqrt{\mathrm{E}}\cdot r_{eff}} & \forall \quad r_{eff} > a_p r_p \end{cases} \tag{9}$$

In the above equations, it may be seen that the target function is used solely as a dependent function in σ_p, via equation (7), and, since the value of the function σ_p is fixed until r_p exceeds r_k, only the post-peak part of the f_s function is actually used in the model.

Overall, the introduction of the SUR function results in changes to two of the model equations presented in Box 1: these being the overall constitutive equation (10) and the expression for the tangent D matrix (11), as follows:

$$\boldsymbol{\sigma} = \left(1 - \omega_p(r_p, r_{eff})\right) \mathbf{D_0} : \boldsymbol{\varepsilon} \tag{10}$$

$$\mathbf{D}_{tan} = \begin{cases} (1-\omega_{pf})\,\mathbf{D_0} & \forall \quad r_{eff} < a_p r_p \\ (1-\omega_{pf})\,\mathbf{D_0} - \dfrac{d\omega_p}{dr_p}\boldsymbol{\sigma}_0 : \left(\mathbf{D_0} \otimes \dfrac{dr_p}{d\boldsymbol{\sigma}}\right)^T & \forall \quad r_{eff} \geq a_p r_p \end{cases} \tag{11}$$

The overall stress-strain relationship (10) now depends on ω_p, rather than ω, which in turn is governed by the value of SUR function σ_p.

The new form of the matrix $\mathbf{D}_{tan}$ is evaluated using the SUR function and therefore is always positive definite. However, this means that $\mathbf{D}_{tan}$ is not the exact tangent when there is loading with respect to the damage function. The implications of this are illustrated in the examples given in Section 5.

4: Predictive function

The one dimensional problem shown in figure 2 was used to provide a first indication of the convergence properties of the SUR approach. This problem comprises a one-dimensional bar, fixed at one end and loaded by prescribed displacement at the other end. A prescribed displacement (u_x) of 0.2 mm was applied evenly over 40 increments. The bar was divided into 3 linear elements of equal length, with the middle element being assigned a small amount of initial damage such that damage only occurred in this central element.

The material properties used for the analysis were: Young's modulus (E=20000 MPa), Poisson's ratio (υ=0.2), tensile strength (f_t=2.5 MPa) and the fracture energy (G_f= 0.1 N/mm).

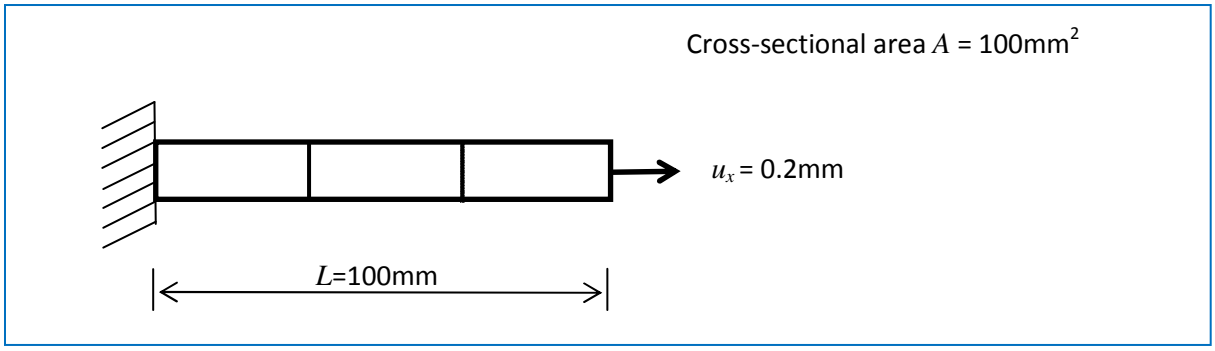

Figure 2: 1-D bar subjected to 0.2 mm prescribed displacement.

Figure 3 shows the number of iterations required to achieve convergence to a tolerance of 10^{-6}, based on an L2 out of balance force norm (Ψ_f). This shows that the 'most difficult' increment was number 3, i.e. the increment that required the greatest number of iterations to achieve convergence.

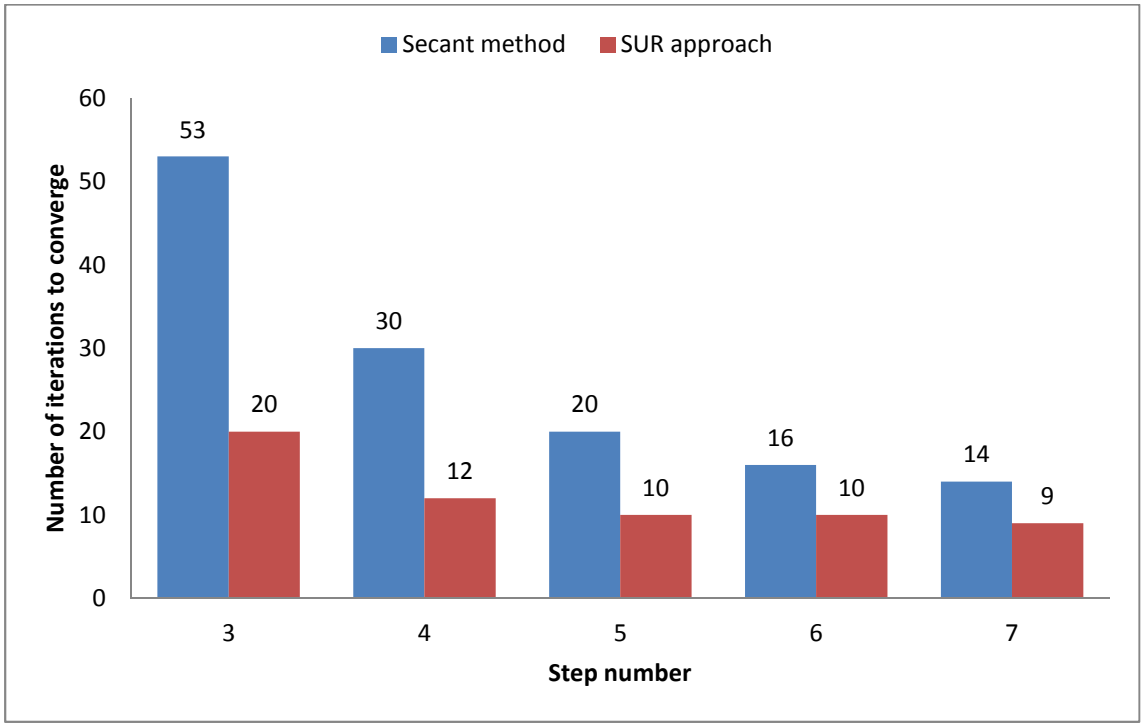

Figure 3: Number of iterations to achieve convergence for the most difficult increments.

In figure 4, the iterative change in the damage evolution parameter (Δr_p) is plotted against the iteration number in semi-log space. It can be seen from this graph that, after a certain point, Δr_p exhibits a linear decay in semi-log space.

The observation that log(Δr_p) reaches a linear decay line led to the development of an algorithm for the prediction of r_p, which was subsequently tested using the examples described in Section 5.

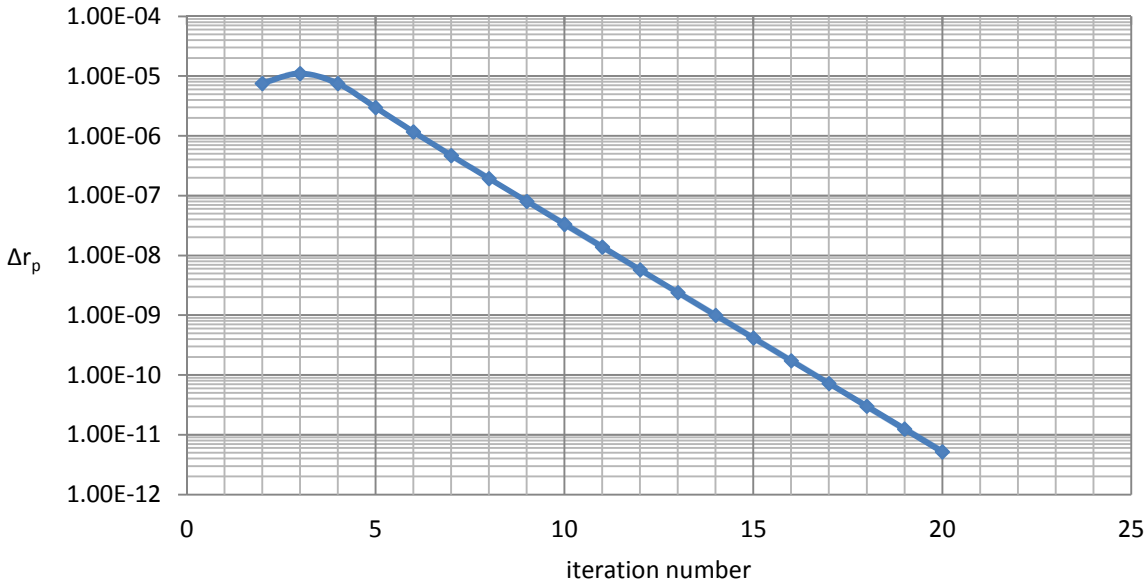

Figure 4: Relationship between number of iterations at the most difficult step (step No. 3) and the differences between damage evolution parameters for 1D-bar.

The predictive function is based on two main principles:

1. The relationship between the number of iterations (*it*) within an increment and the iterative change of the damage evolution parameter ($\Delta r_{p_i} = r_{p_{it}} - r_{p_{it-1}}$) decays linearly in semi-log space, once stable convergence has been achieved, as shown in figure 5.

2. When the slope of the *it* vs $log(\Delta r_p)$ curve starts decreasing (see figure 4), a trial prediction of the damage evolution parameter (r_{pp}) can be computed using equation (14). Once the normalised difference between two consecutive predictions is less than 5%, r_p is set to the most recently computed trial value, i.e. $r_p = r_{pp}$.

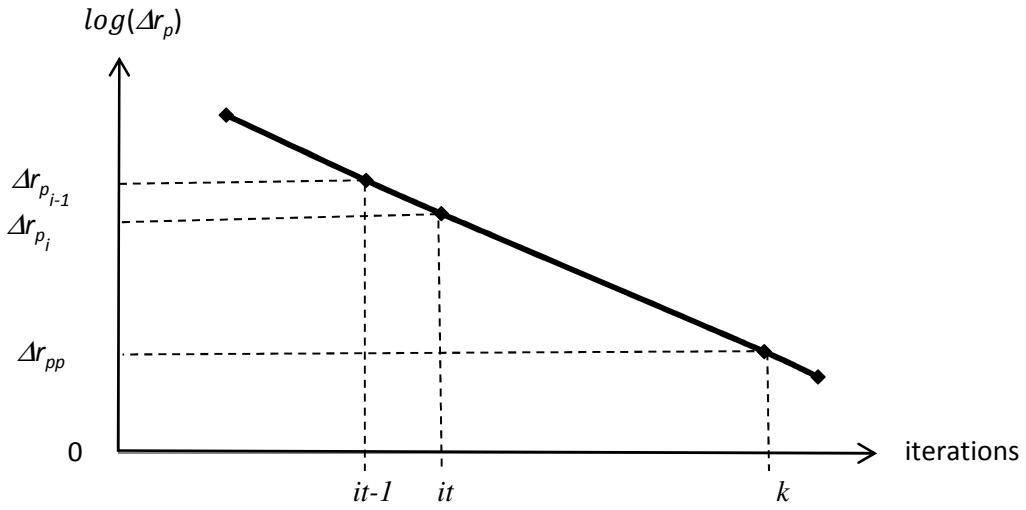

Figure 5: Relation between number of iterations and differences between damage evolution parameters within a time step.

Based on figure (5), the following extrapolation can be obtained:

$$\frac{log\left(\Delta r_{p_i}\right)-log\left(\Delta r_{p_{i-1}}\right)}{1}=\frac{log\left(\Delta r_{pp}\right)-log\left(\Delta r_{p_i}\right)}{k-it} \tag{12}$$

Equation (12) can be simplified to:

$$\Delta r_{pp}=10^{j\cdot b+a}$$

in which $j=k-it$, $b=log\left(\Delta r_{p_i}\right)-log\left(\Delta r_{p_{i-1}}\right)$ and $a=log\left(\Delta r_{p_i}\right)$.

It follows that the predicted damage evolution parameter is;

$$r_{pp}=r_{p_{it}}+\sum_{j=1}^{\infty}\Delta r_{pp_j} \tag{13}$$

The summation in equation (13) may also be written;

$$\sum_{j=1}^{\infty}\Delta r_{pp_j}=\frac{10^a(10^b-10^{b\infty})}{1-10^b}$$

The prediction is only considered when Δr_p is reducing and this means that b always satisfies $b < 0$, and therefore $10^{b\infty}=0$. The predictive damage evolution parameter r_{pp} can now be written:

$$r_{pp} = r_{p\,it} + \frac{\Delta r_{p_i}^{\,2}}{\Delta r_{p_{i-1}} - \Delta r_{p_i}} \tag{14}$$

Box 2 summarises the steps involved in computing the r_p prediction.

Box 2: Predictive function algorithm		
r_{pp_i}	if $\Delta r_{p_i} < \Delta r_{p_{i-1}}$	Compute 1st r_p prediction at it
$r_{pp_{i+1}}$	if $\Delta r_{p_{i+1}} < \Delta r_{p_i}$	Compute 2nd r_p prediction at $it+1$
$r_p = r_{pp_{i+1}}$	if $\frac{r_{pp_{i+1}} - r_{pp_i}}{r_{pp_{i+1}}} \leq 5\%$	Set r_p value to $r_{pp_{i+1}}$, if the second principal is satisfied

The predictive algorithm has been derived from the response of a 1D three element example and relies on the iterative solution reaching a point at which the change in the damage evolution parameter exhibits the semi-log decay shown in figure 4 for all active damage zones. The point at which this semi-log decay occurs will be problem dependent and may be expected to be reached in fewer iterations in small 1D problems than in larger multi-element 2D and 3D cases. This issue is explored in the next section of this paper which assesses the performance of the predictive algorithm for range of multi-element 1D and 2D problems.

5: Numerical examples

Five numerical examples are used to illustrate the performance of the proposed SUR approach for the non-linear FE analysis of QB structures. The purpose of the study is not to examine the accuracy of the isotropic damage model and its ability to simulate the behaviour of QB materials in a FE context, which has been established elsewhere [33, 34], but rather to illustrate the convergence characteristics of the SUR approaches and illustrate their potential benefits. Therefore, the examples were chosen for their numerical characteristics and are not all based upon real experiments or structures.

The first example considers the 1D bar problem described in section 4 (see figure 2). The second example is a 2D notched fracture specimen, loaded by prescribed displacement along its upper boundary, as shown in figure 9. The third example is based on the reinforced concrete prism tested by Elfgren and Noghabai [37]. The forth example is a 2D double notched specimen subject to mixed mode loading by prescribed displacement, as illustrated in figure 25 . The final example adopts the same configuration as used in example 2 but with larger dimensions (see figure 31). However, this example is only used to explore the effect of varying the two main parameters of SUR function on the convergence performance of the solution. The material parameters used for all examples are given in table 1. All 2D meshes comprised bilinear isoparametric elements.

Examples 1 to 4 are considered with the following three approaches:

- Secant method
- SUR approach
- Predictive-SUR approach

Table 1: Concrete material properties and convergence tolerances

Ex	E_c (GPa)	E_s (GPa)	υ	f_t (MPa)	G_f (N/mm)	Ψ_d (%)	Ψ_f (%)
5.1	20	-	0.20	2.5	0.10	0.1 & 0.0001	0.1 & 0.0001
5.2	20	-	0.20	2.5	0.10	0.10 & 0.0001	0.10 & 0.0001
5.3	42	200	0.20	2.5	0.10	0.10	0.10
5.4	20	-	0.20	2.5	0.10	0.10	0.10
5.5	30	-	0.20	2.5	0.10	0.10	0.10

In all examples, the loading was monotonic and consistent convergence parameters were used for all analyses within an example. Thus, the form of the unloading-reloading curve would not be

expected to affect the overall predicted response but only to affect the convergence characteristics. The former was indeed the case, as may be seen from the load-displacement responses given below.

Convergence of the incremental-iterative solutions was based on the decay of both the L2 iterative displacement and out of balance force norms, i.e. the convergence of both of these norms was achieved for all steps of every solution. Two levels of convergence tolerance have been used in the examples: the first being a tolerance of 0.1%, which is considered adequate for all practical analyses. The second tolerance of 0.0001% is used in the first two examples to explore the convergence characteristics beyond the first limit. The latter was not used in all examples because, (i) the results show that there is no appreciable difference in the results from a solution with a 0.1% limit compared with those obtained using 0.0001% tolerance, and (ii) the very high number of iterations required by the reference 'secant' solution made full comparisons difficult to obtain for the later examples.

In these examples, the solution characteristics are illustrated by showing the number of iterations required to achieve convergence for selected increments. In all cases, the increments chosen are those which required the most iterations to achieve convergence and are thus are termed 'difficult increments'

Example 5.1: One-Dimensional tensile test

The 1D bar problem considered in this example was loaded to a prescribed displacement of 0.2mm in even increments. Two sets of analyses were undertaken, one in which the prescribed displacement was applied over 40 increments and the other in which 100 increments were used. In addition, both sets of analyses were carried out with 0.1% and 0.0001% convergence tolerances.

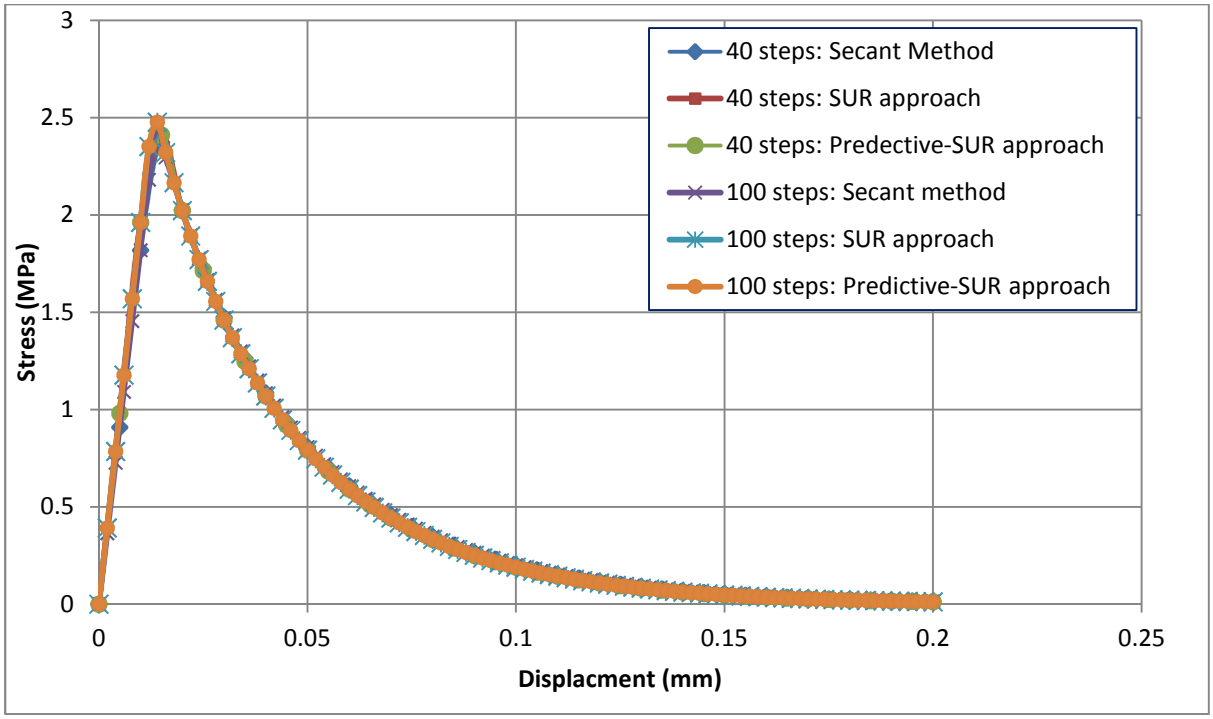

Figure 6: Displacement-stress relationship for the 1D bar with 40 and 100 increments.

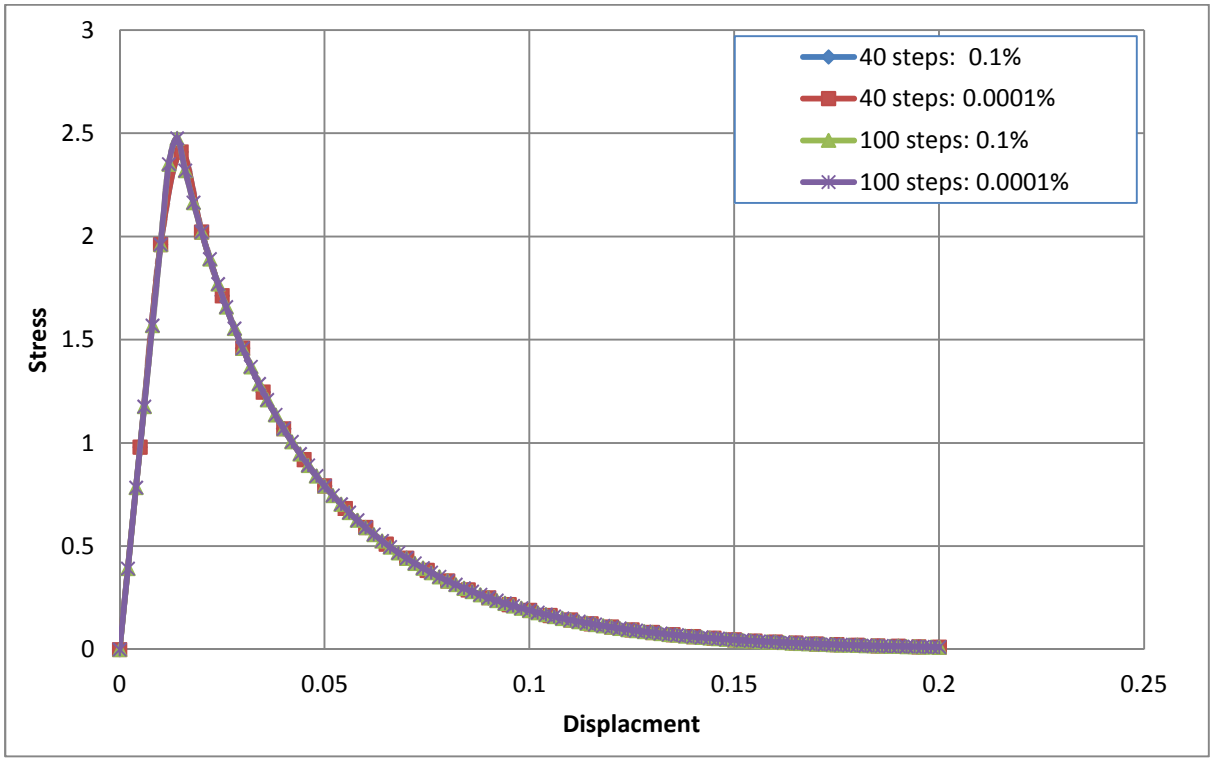

Figure 7: Displacement-stress relationship for the 1D bar using SUR approach with 10^{-3} and 10^{-6} convergence tolerances.

The resulting stress-displacement responses from the two sets of analyses are shown in figure 6 and, as expected, the results from the various analyses are indistinguishable from each other. This is also the case for the results obtained using the different convergence tolerances of 10^{-3} and 10^{-6}, as can be seen in figure 7.

Figures 8,9,10 and 11 present the number of iterations required to achieve convergence at the most difficult steps. In all sets of analyses, the SUR and predictive SUR approaches achieved converged solutions with far fewer iterations than the secant method.

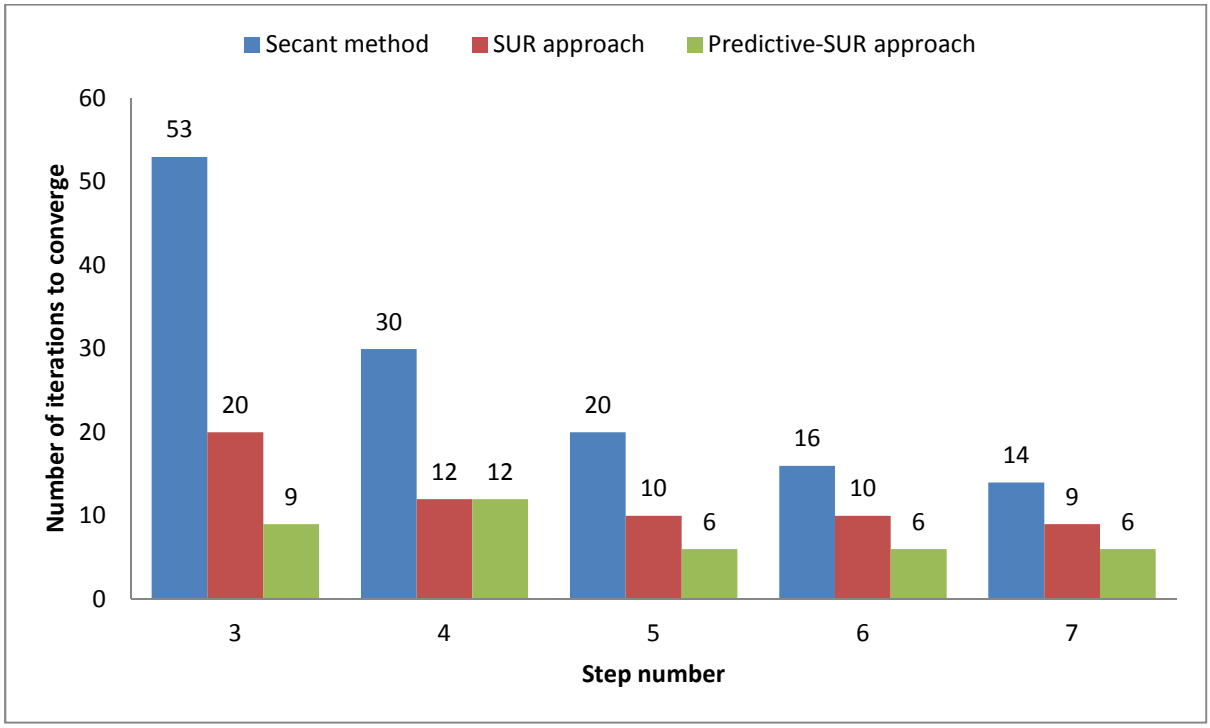

Figure 8: Number of iterations to achieve convergence for the most difficult increments for 1D bar with 40 increments (convergence tolerance=10^{-6}).

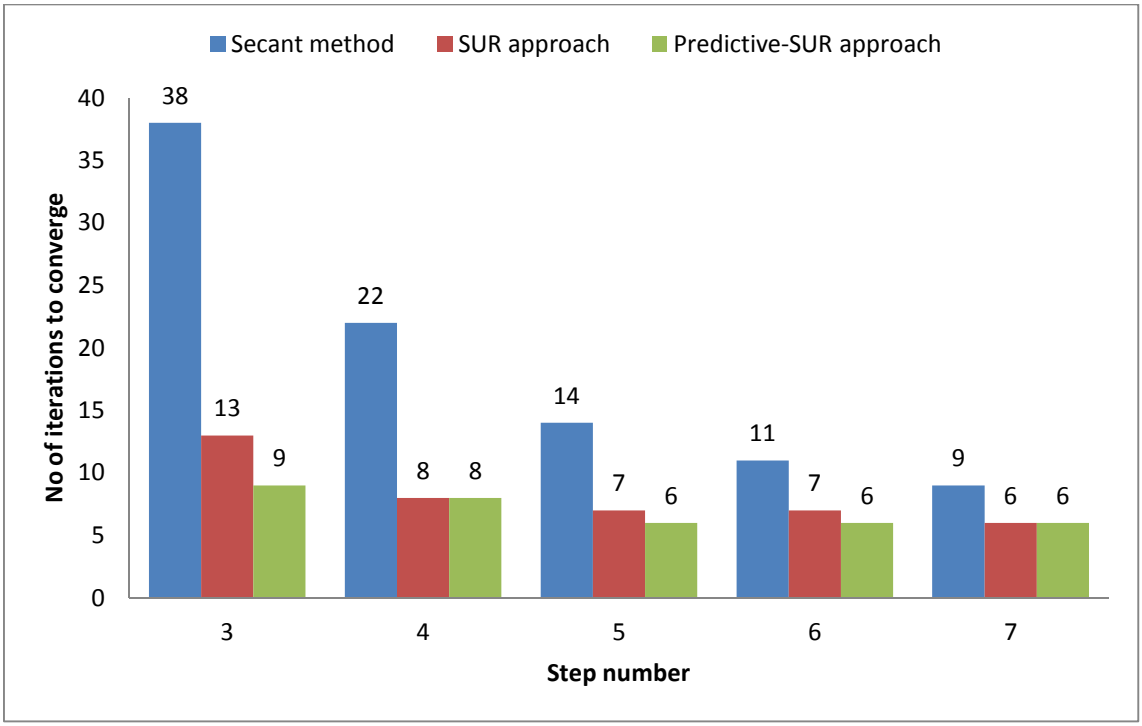

Figure 9: Number of iterations to achieve convergence for the most difficult increments for 1D bar with 40 increments (convergence tolerance=10^{-3}).

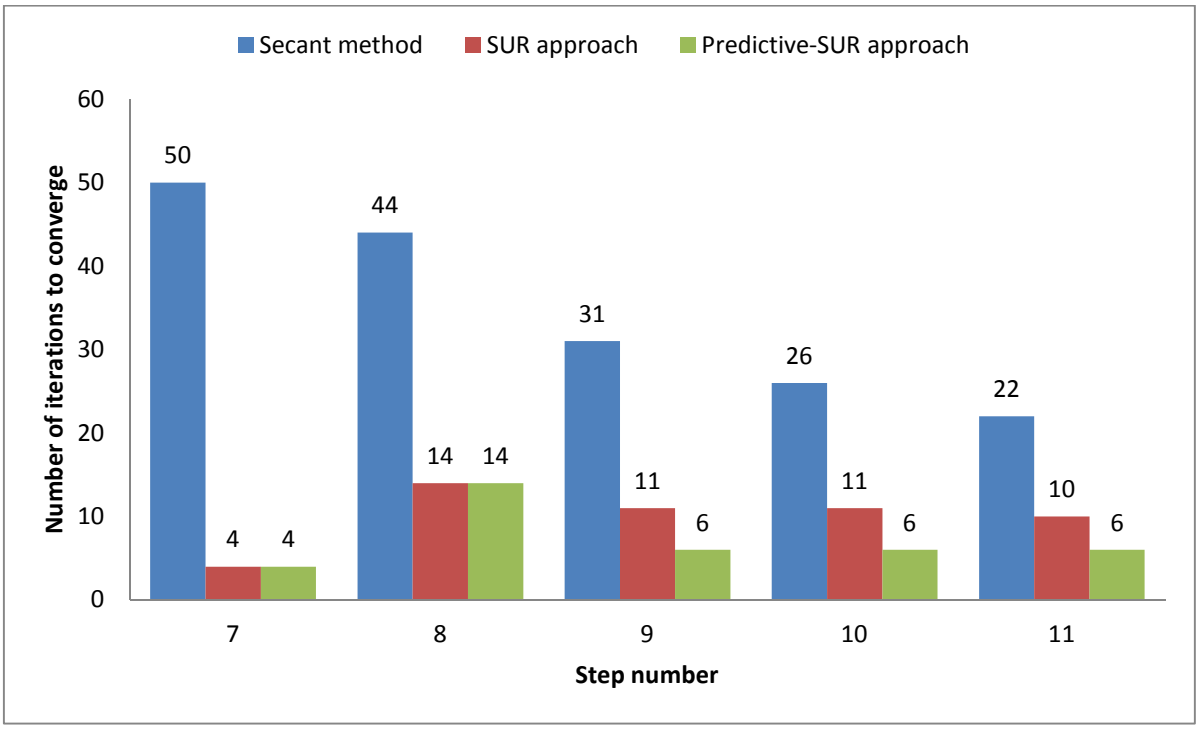

Figure 10: Number of iterations to achieve convergence for the most difficult increments for 1D bar with 100 increments (convergence tolerance=10^{-6}).

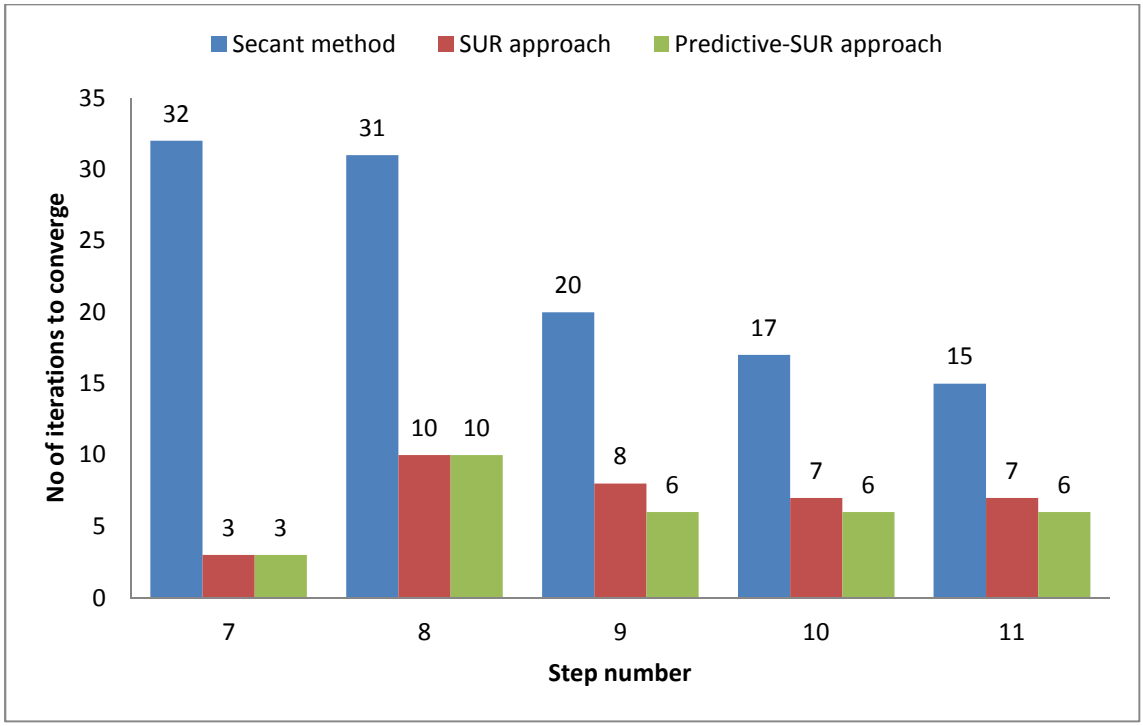

Figure 11: Number of iterations to achieve convergence for the most difficult increments for 1D bar with 100 increments (convergence tolerance=10^{-3}).

Example 5.2: Two-Dimensional plane stress specimen

The idealised 2-D structure considered in this example is discretised with the coarse and fine meshes shown in figure 13. The analysis was undertaken using 2 different prescribed displacement increments, one using 50 steps and the other 100 steps. Also, two convergence tolerances 10^{-3} and 10^{-6} were used for the analysis.

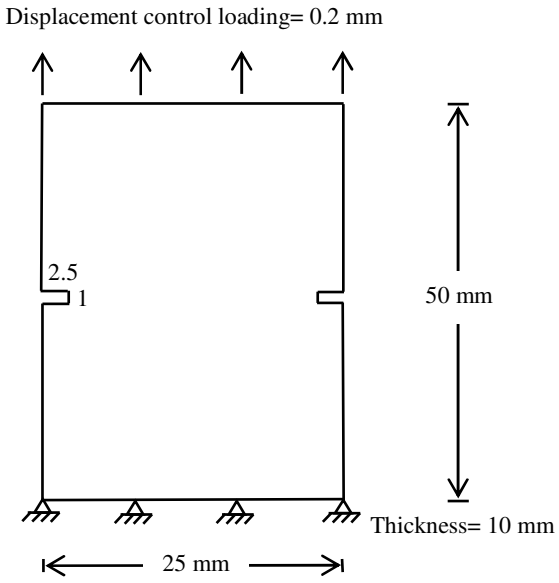

Figure 12: Dimension of the 2D notched plane stress example.

Exaggerated deformed mesh plots are given in figure 14. The numerical load displacement responses from the analyses using the three approaches with Mesh1 and Mesh2 using 50 and 100 steps are shown in figures 15 and 16. Also, the stress-displacement responses for Mesh1 using the SUR approach for two convergence tolerances 10^{-3} and 10^{-6} are presented in figure 17 .In addition, a comparison between the number of iterations needed for the three solutions to converge at the most difficult steps can be seen in figures 18, 19, 20, 21, 22, 23, 24 and 25. The increments requiring the most iterations are those associated with crack initiation and early crack propagation. These normally coincide with the peak and early post-peak sections of the overall response curve.

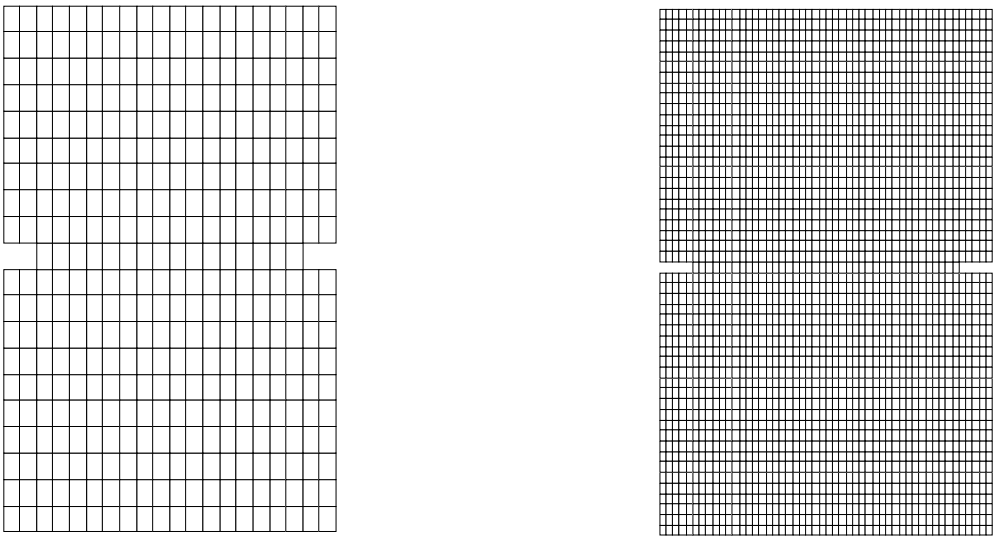

Mesh1 Mesh2

Figure 13: Finite Element Meshes.

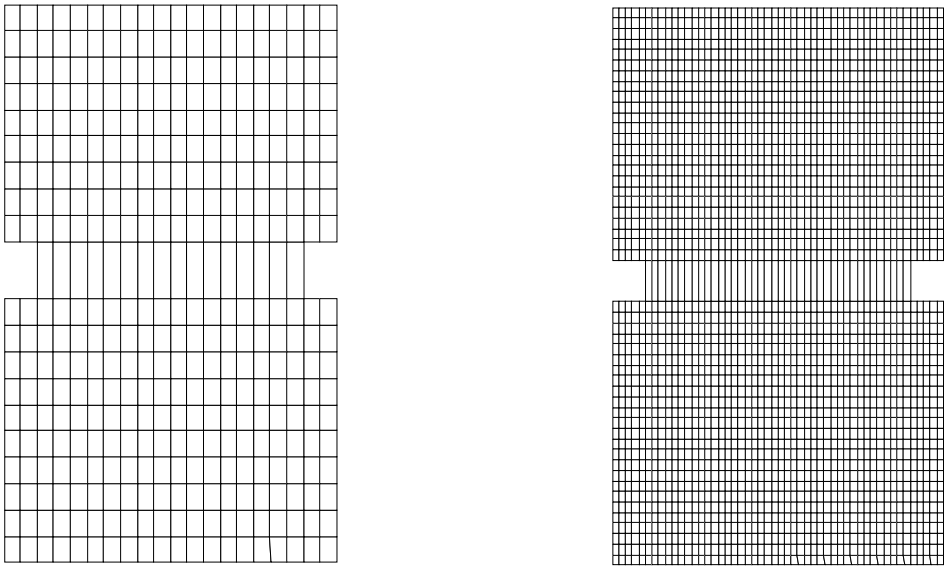

Figure 14: Exaggerated deformed mesh plots at final increment for Mesh1 and Mesh2.

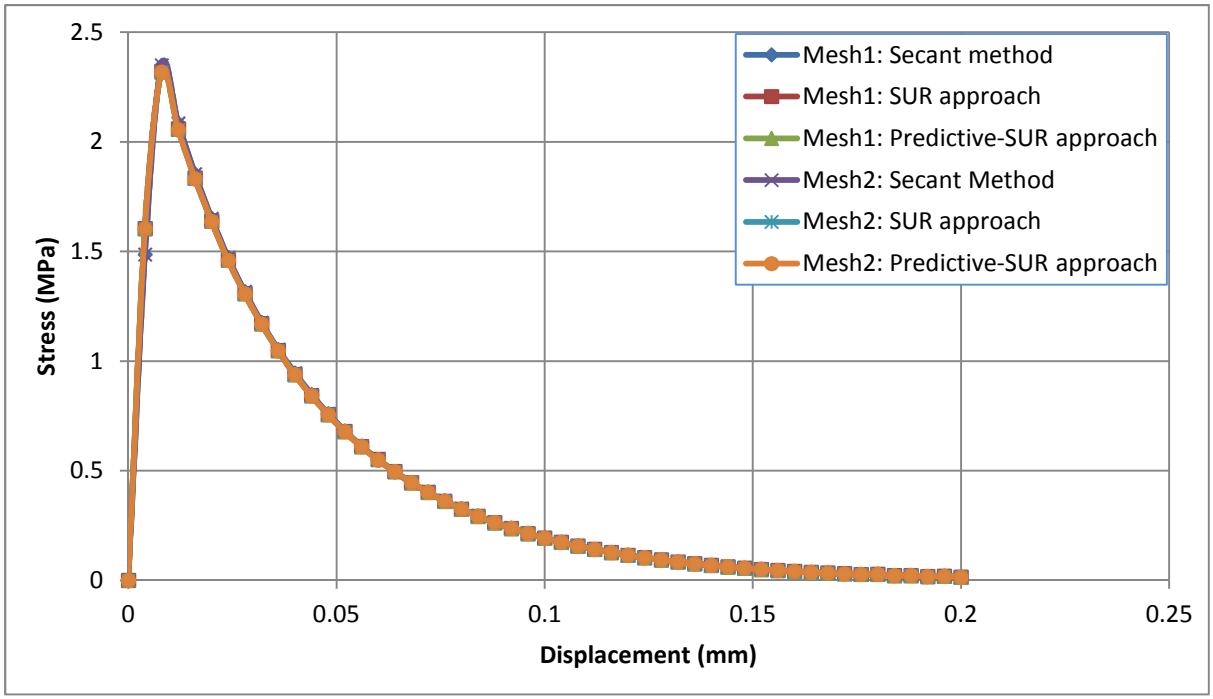

Figure 15: Displacement-Stress relationship for 2D plane stress example with 50 steps.

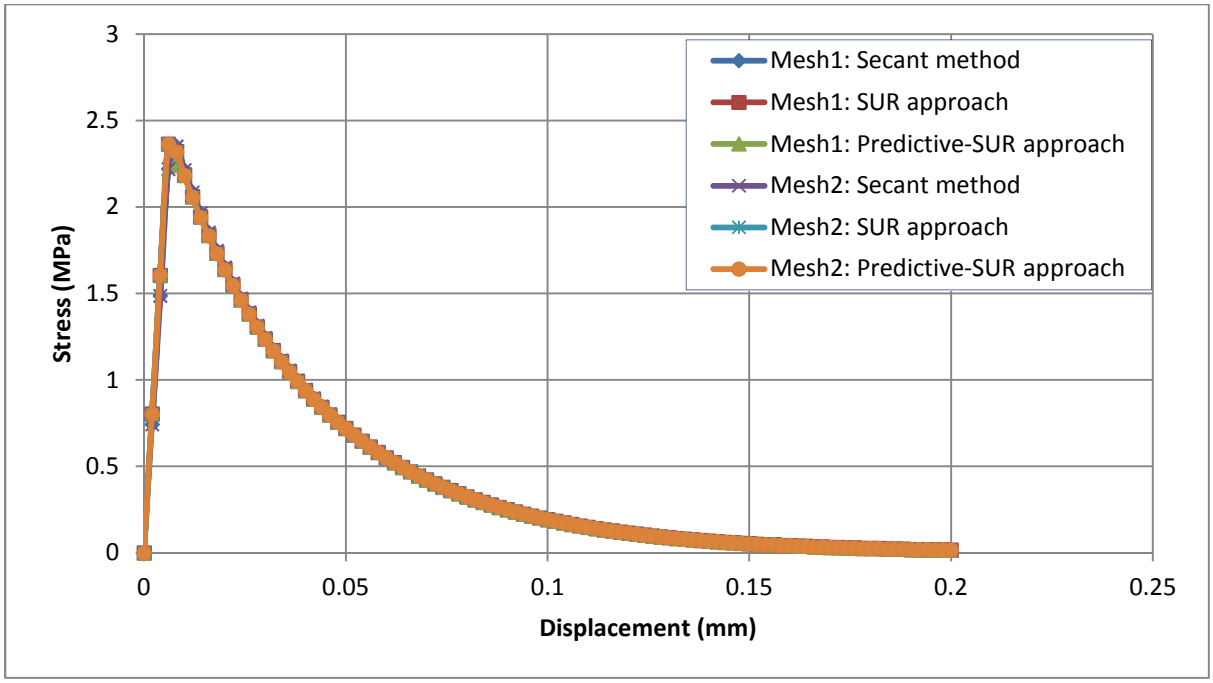

Figure 16: Displacement-Stress relationship for 2D plane stress example with 100 steps.

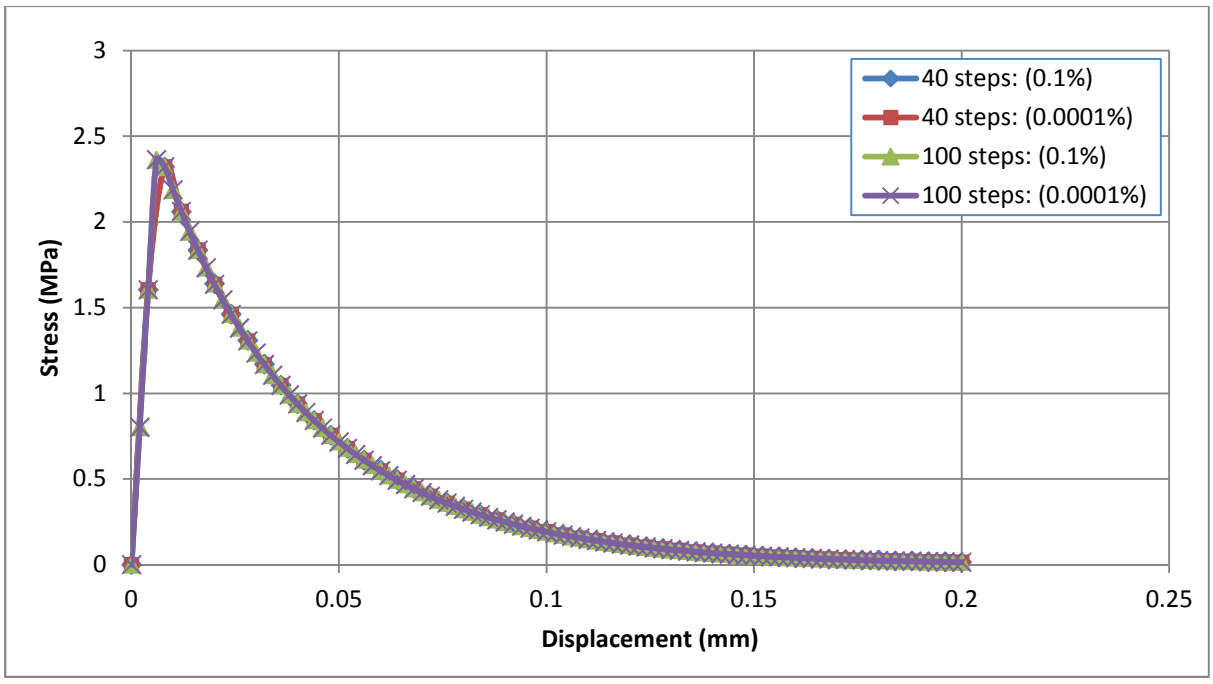

Figure 17: Displacement-Stress relationship for Mesh1 using SUR approach with convergence tolerances ($10^{-3}$and 10^{-6}).

As in Example 1, the stress-displacement results obtained with both convergence tolerances (10^{-3} and 10^{-6}) are indistinguishable from each other, as can be seen in figure 17.

As with example 1, the savings gained by using the SUR approaches are considerable, although in this case there is little difference between the basic SUR and the predictive-SUR solutions.

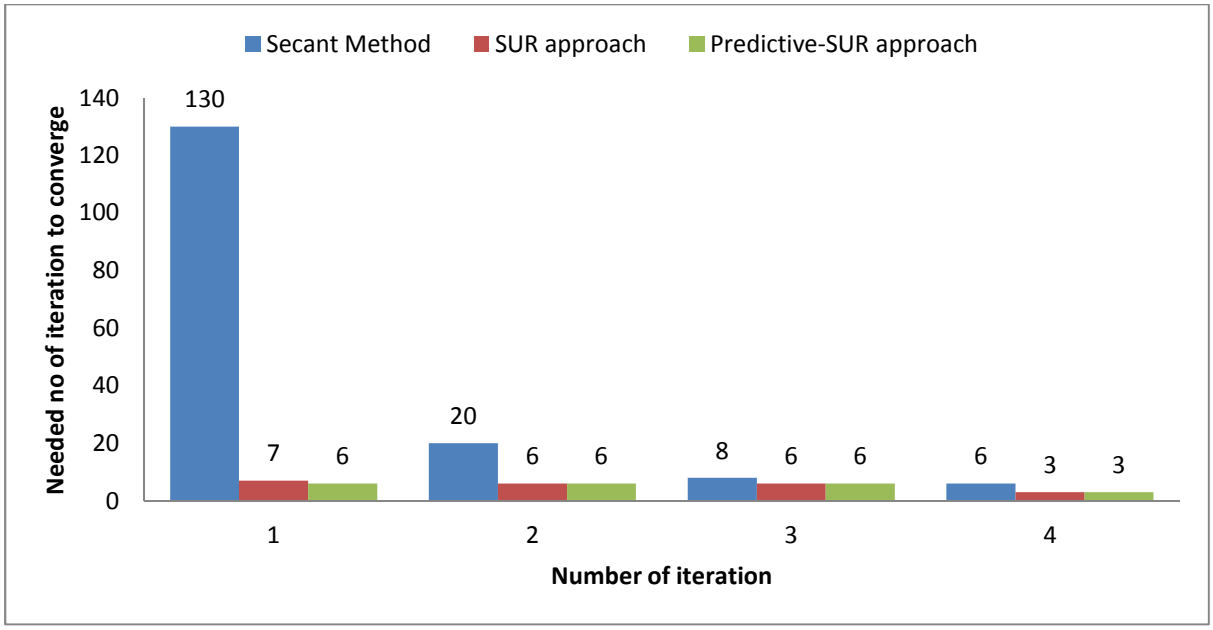

Figure 18: Number of iterations to achieve convergence for the most difficult increments for Mesh1 with 50 increments (convergence tolerance=10^{-3}).

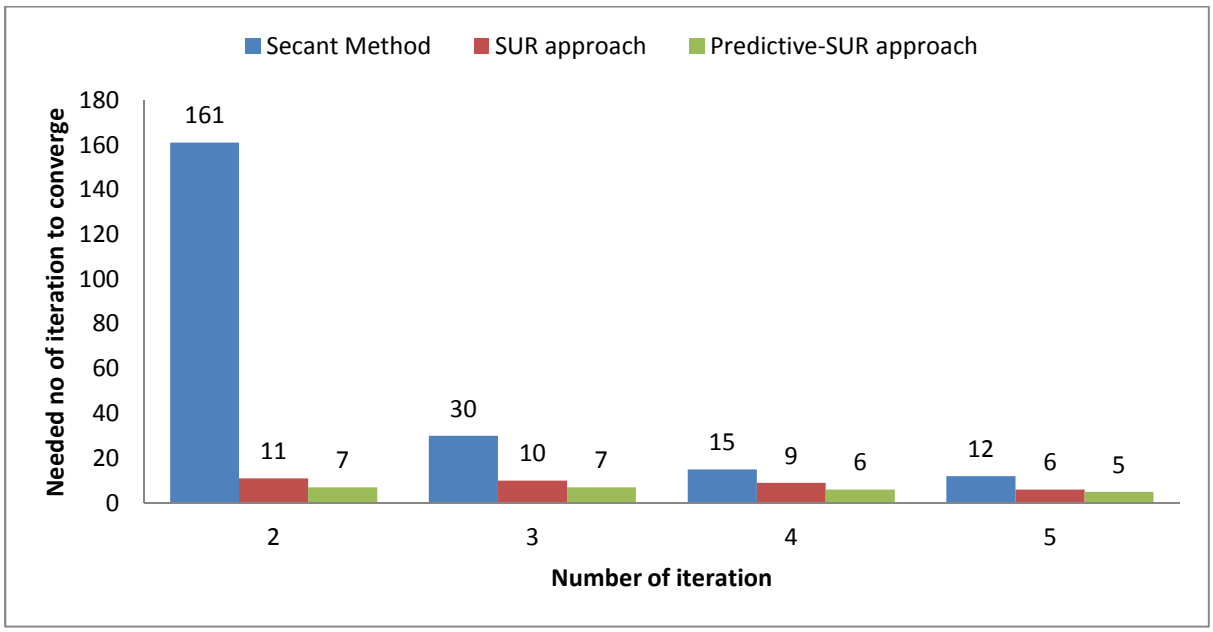

Figure 19: Number of iterations to achieve convergence for the most difficult increments for Mesh1 with 50 increments (convergence tolerance=10^{-6}).

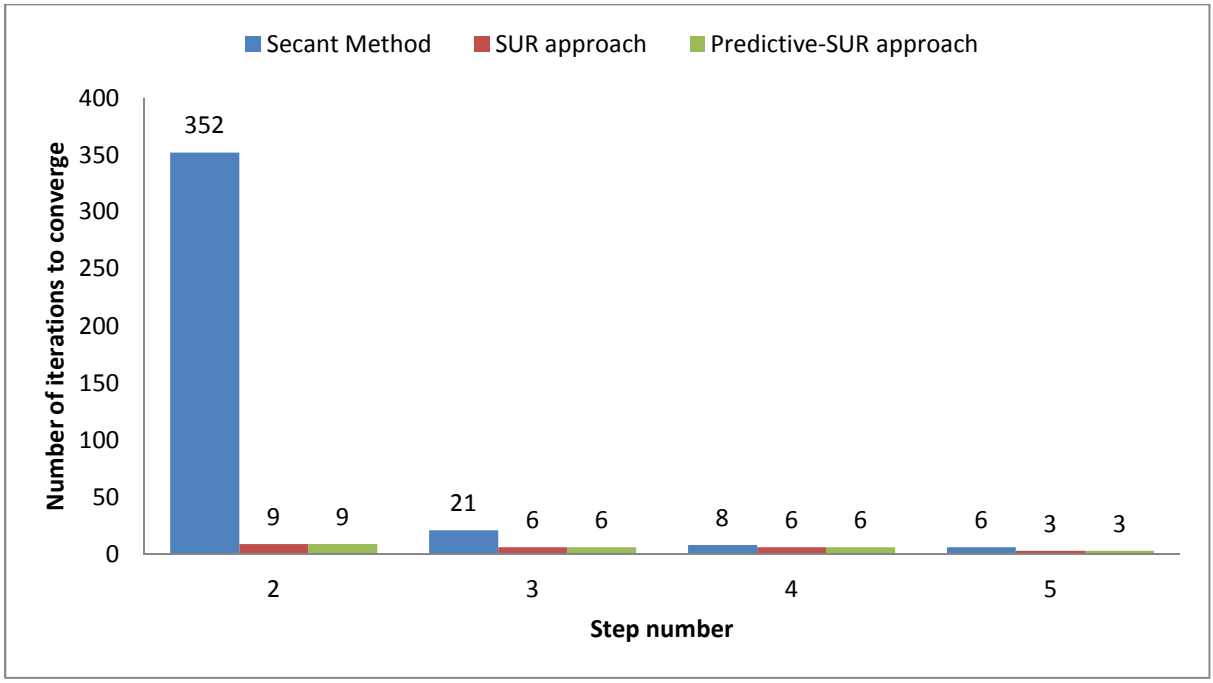

Figure 20: Number of iterations to achieve convergence for the most difficult increments for Mesh2 with 50 increments (convergence tolerance=10^{-3}).

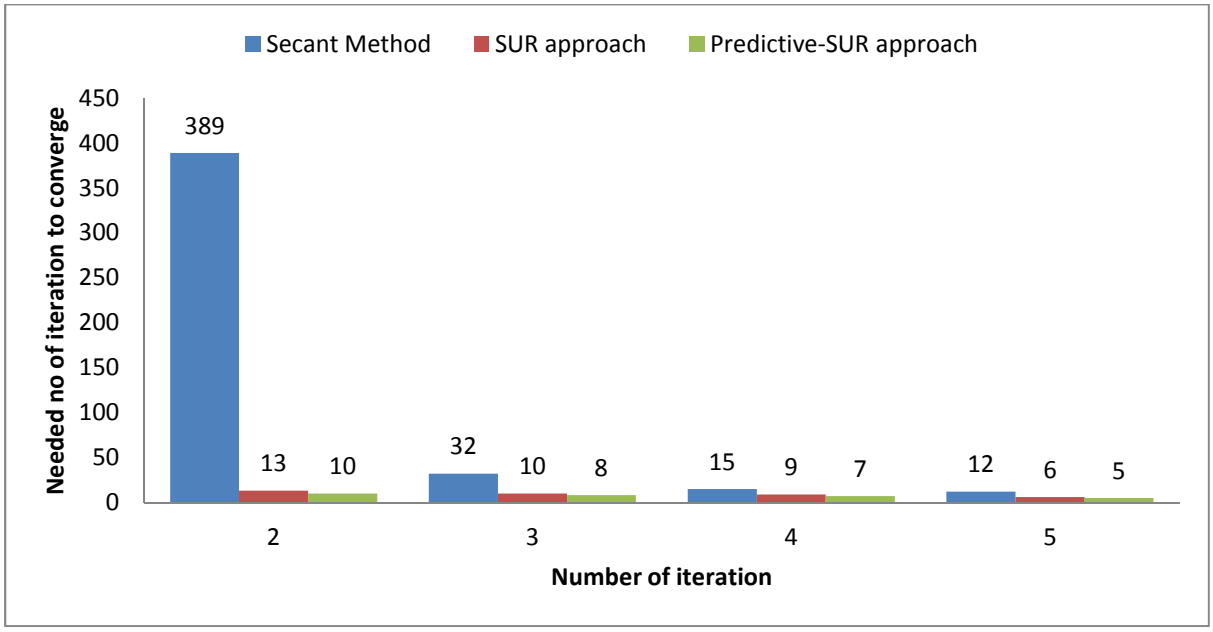

Figure 21: Number of iterations to achieve convergence for the most difficult increments for Mesh2 with 50 increments (convergence tolerance=10^{-6}).

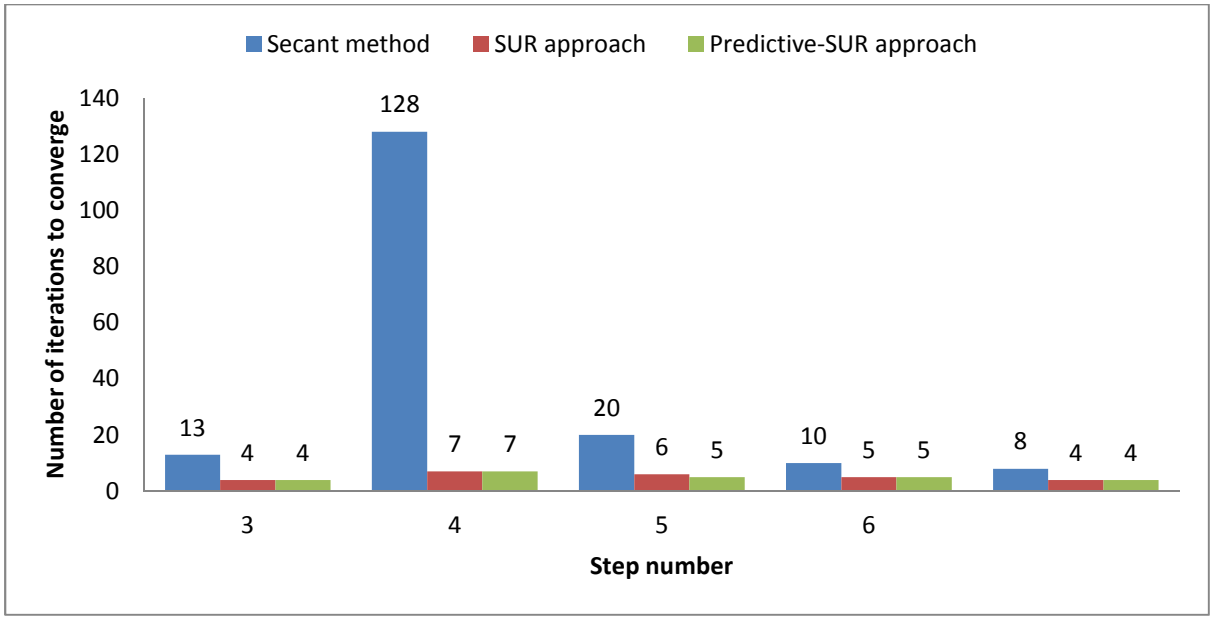

Figure 22: Number of iterations to achieve convergence for the most difficult increments for Mesh1 with 100 increments (convergence tolerance=10^{-3}).

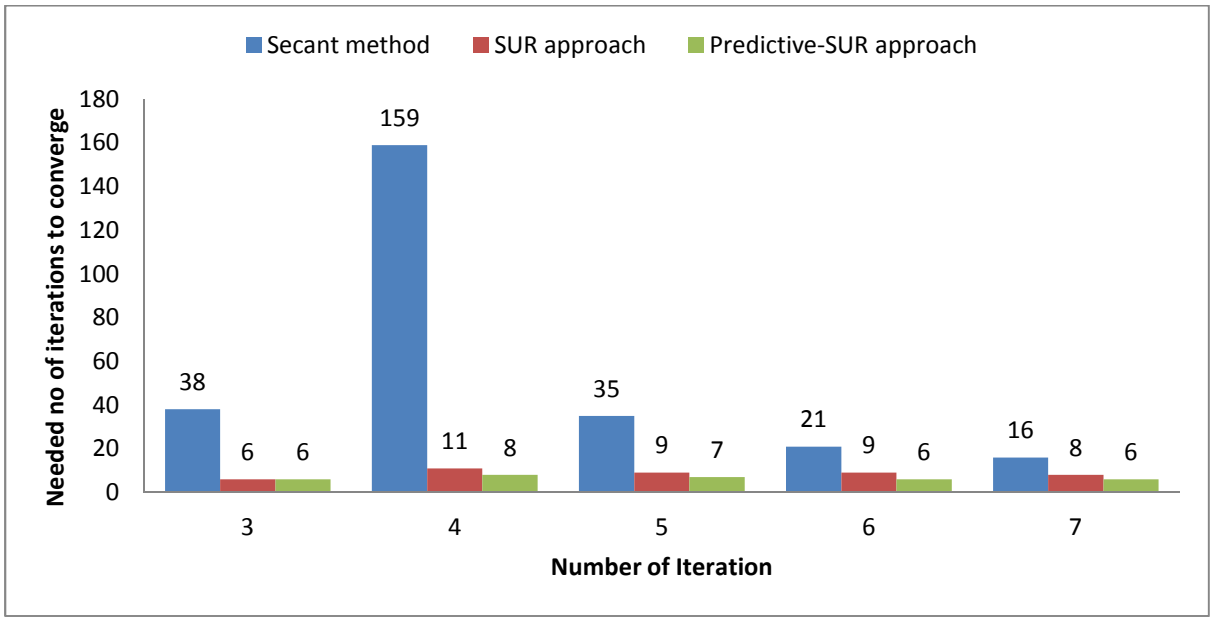

Figure 23: Number of iterations to achieve convergence for the most difficult increments for Mesh1 with 100 increments (convergence tolerance=10^{-6}).

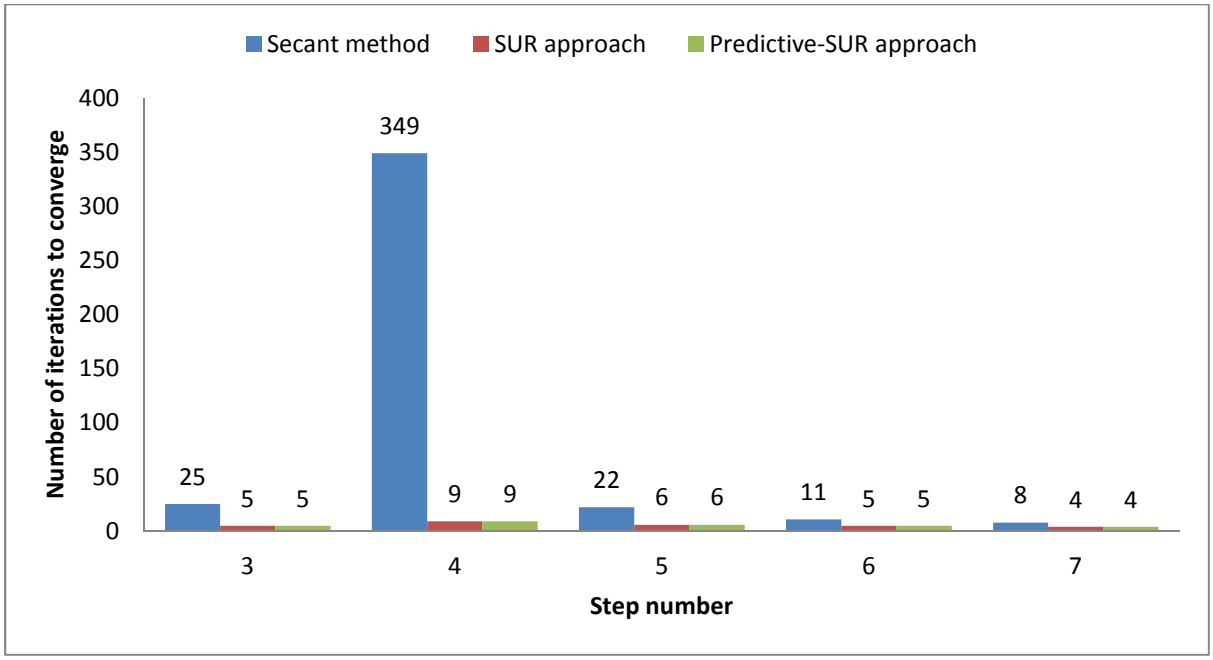

Figure 24: Number of iterations to achieve convergence for the most difficult increments for Mesh2 with 100 increments (convergence tolerance=10^{-3}).

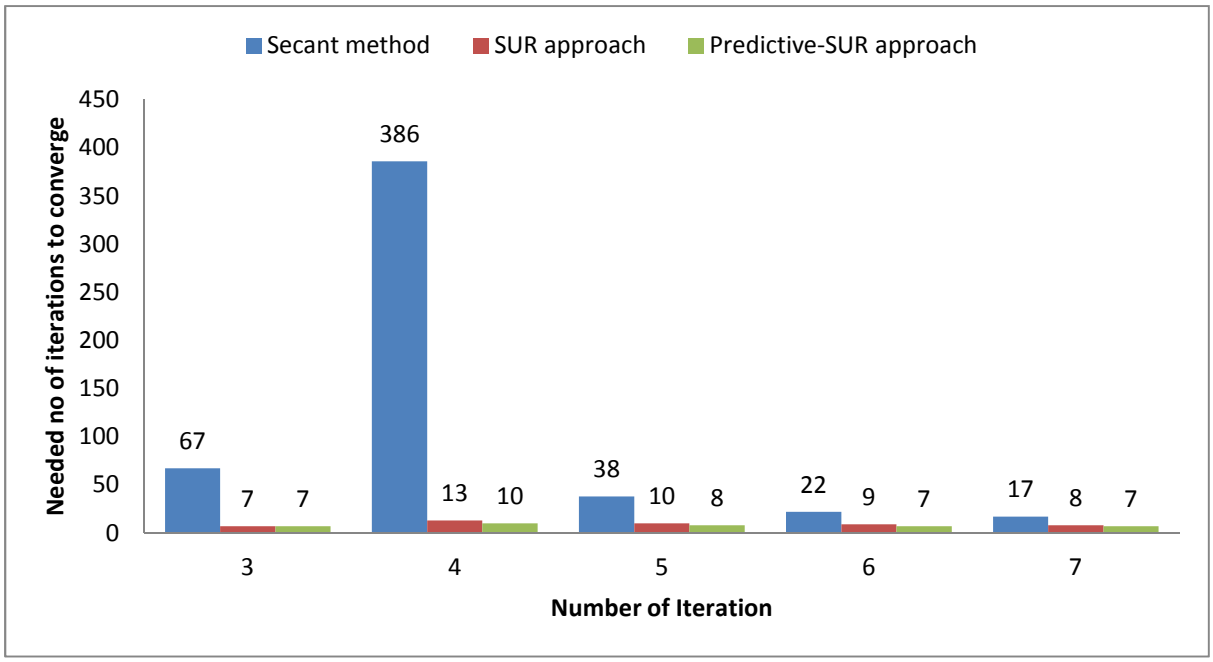

Figure 25: Number of iterations to achieve convergence for the most difficult increments for Mesh2 with 100 increments (convergence tolerance=10^{-6}).

Example 5.3: Reinforced Concrete Prism

The RC specimen considered in this example was reinforced with a single central reinforcement bar, as illustrated in figure 26. The analyses were carried out with 50 and 100 prescribed displacement increments to reach a displacement of 1mm at the load position. The finite element mesh, which represents ¼ of the specimen, is shown in figure 27. The exaggerated deformed mesh plot of the ¼ of the RC prism at the final increment (0.01 mm) is given in figure 28. Furthermore, figures 29 shows a contour plot of the damage parameter, also at the final increment.

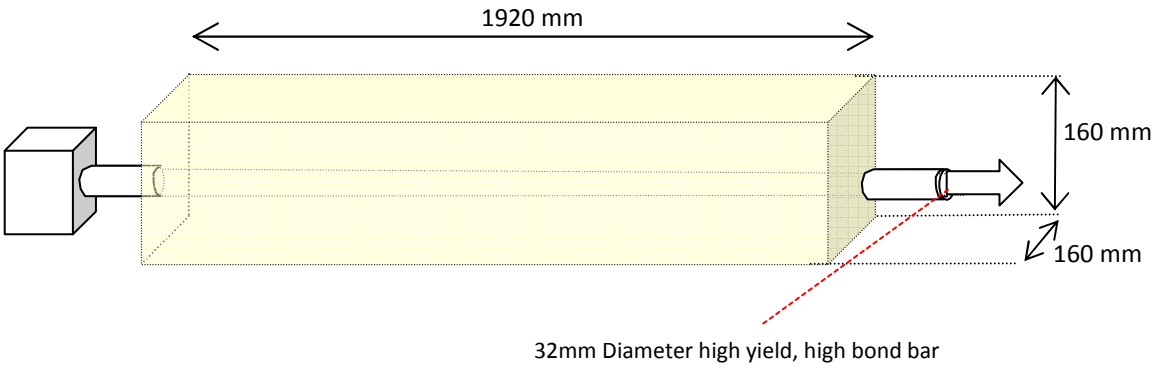

Figure 26: Dimension details for RC prism.

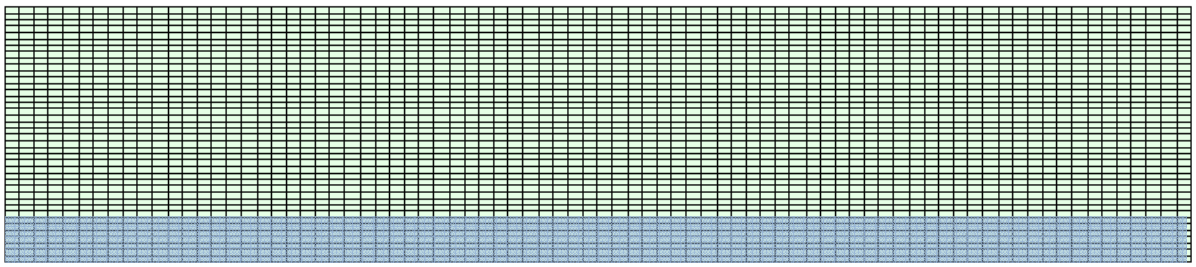

Figure 27: Finite element mesh of RC prism.

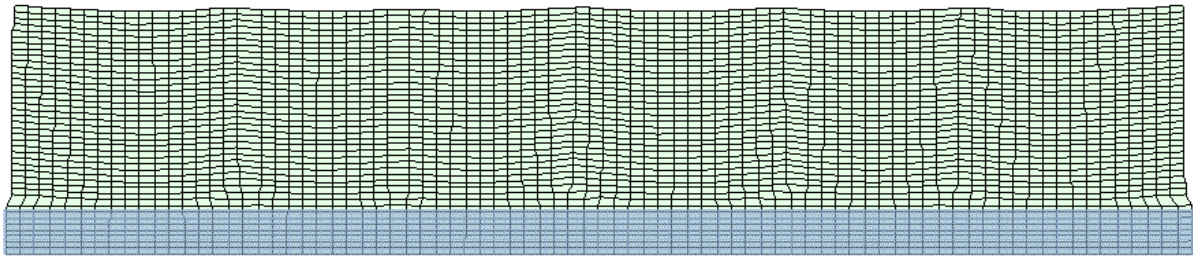

Figure 28: Exaggerated deformed mesh plot at final increment.

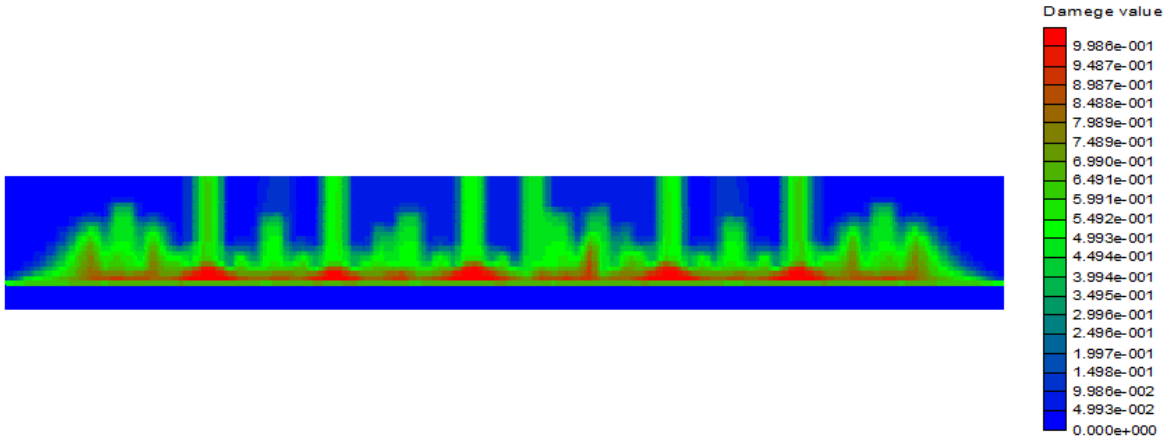

Figure 29: Damage value contour plot at final displacement increment.

Numerical stress-displacement responses from all of the analyses of this specimen are shown in figure 30, in which the average stress is that in the elastic reinforcing bar.

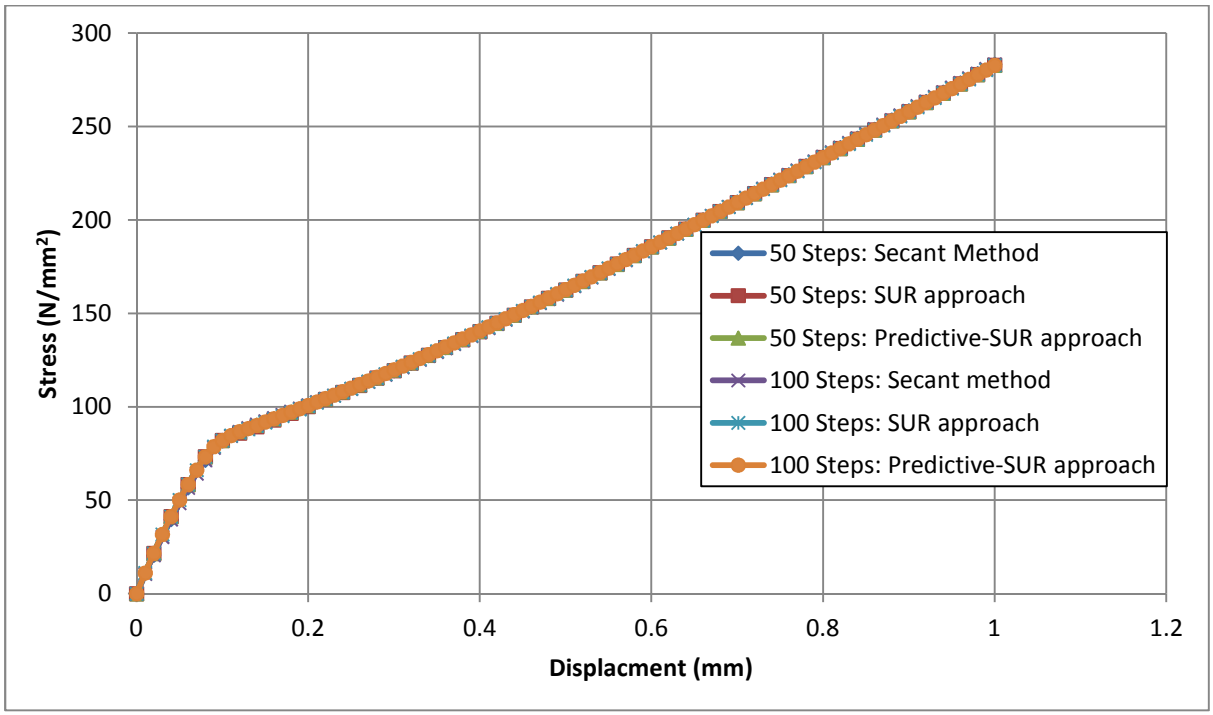

Figure 30: Load-displacement responses of reinforced bar.

The number of iterations required, for both the 50 and 100 step solutions, are presented in figures 31 and 32 respectively. The efficiency of the SUR approaches, relative to the Secant approach, is again evident. The other main observation from these results is that, overall, the SUR-predictive solution uses fewest iterations. However, there are single increments for which the basic SUR solution uses fewer iterations than that predictive-SUR solution. This matter is discussed in Section 6.

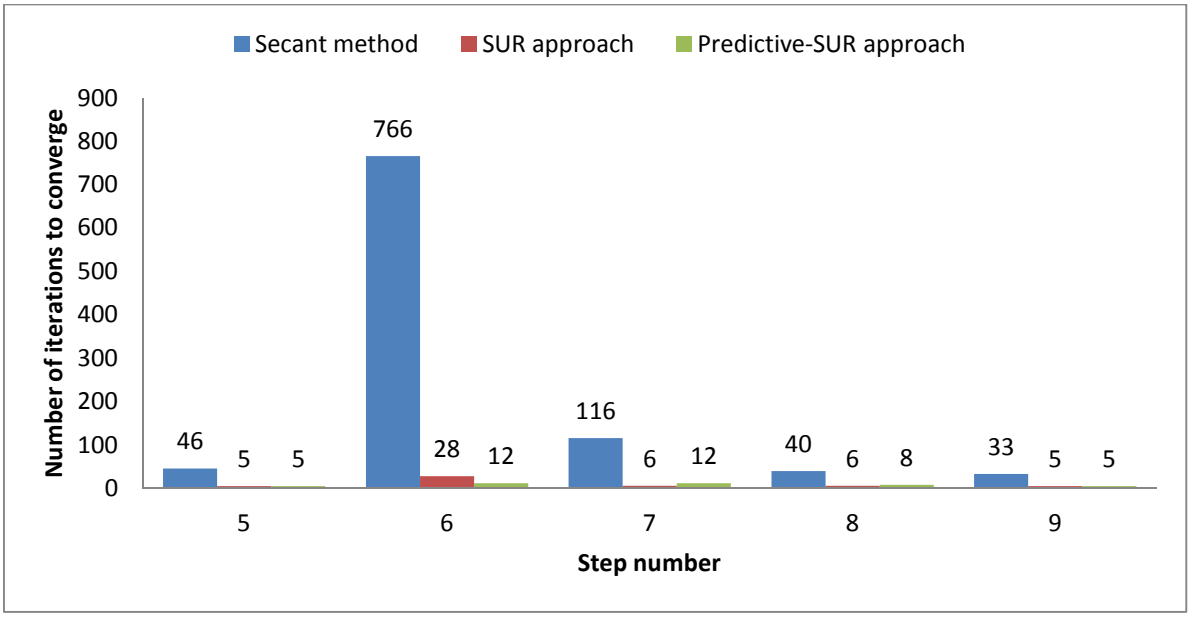

Figure 31: Number of iterations to achieve convergence for the most difficult increments of RC prism with 50 increments.

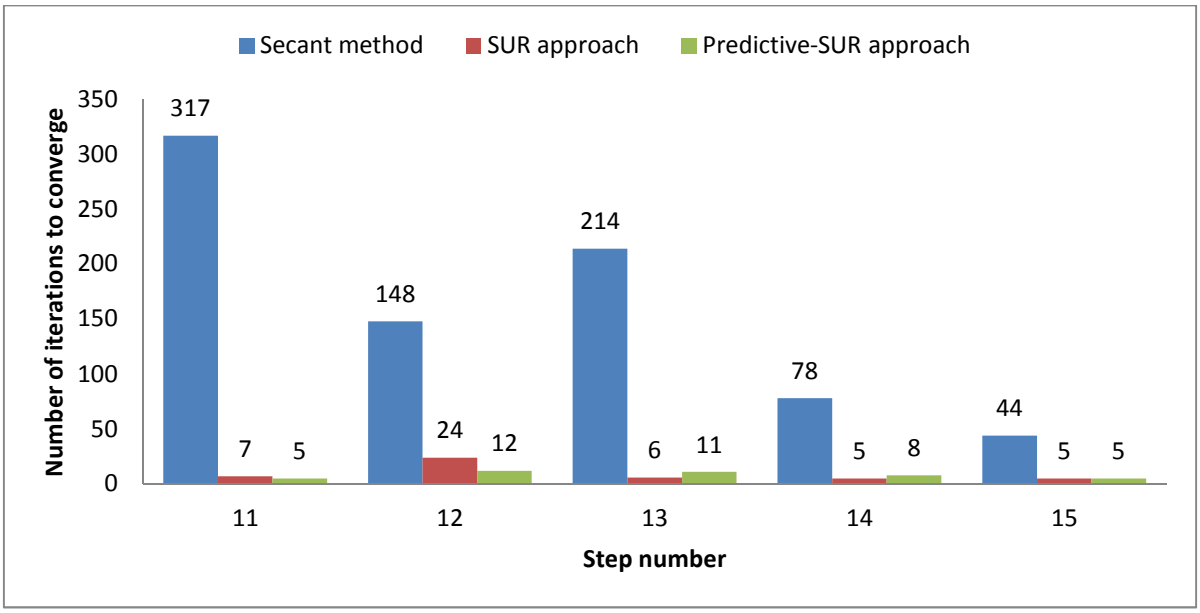

Figure 32: Number of iterations to achieve convergence for the most difficult increments of RC prism with 100 increments.

Example 5.4: 2-D double notched example

Figure 33 shows the 2D double notched specimen used for this example. This is subjected to a combination of shear and tensile loading via prescribed vertical and horizontal displacements. The analyses were undertaken using 40 and 100 prescribed displacement increments. The exaggerated deformed mesh plot of the 2D specimen using 100 steps at the final displacement increment is depicted in figure 34. Also, contour plots of the damage parameter and principal stresses are shown in figures 34 and 35, respectively.

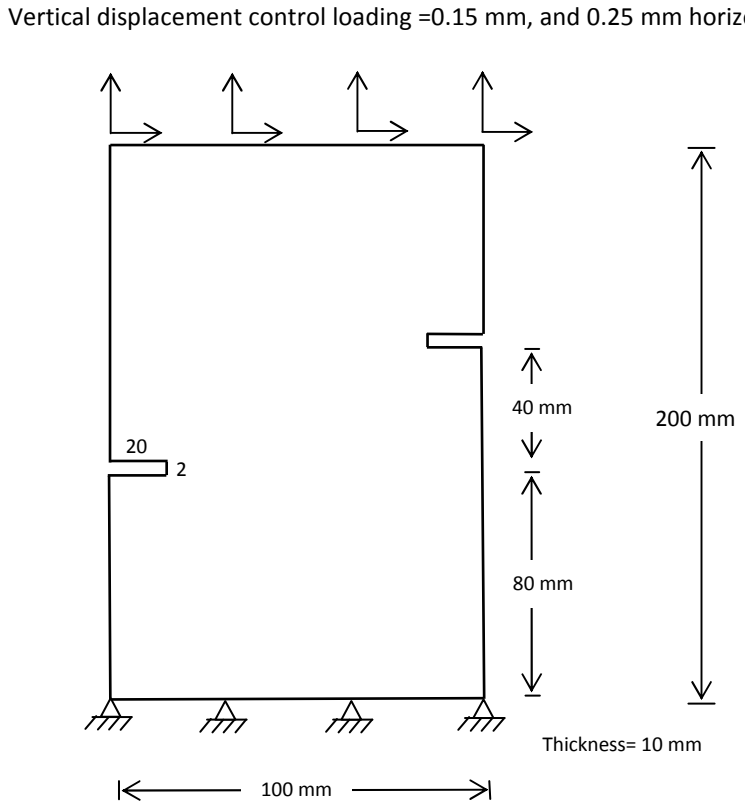

Figure 33: dimensional details of double notched specimen

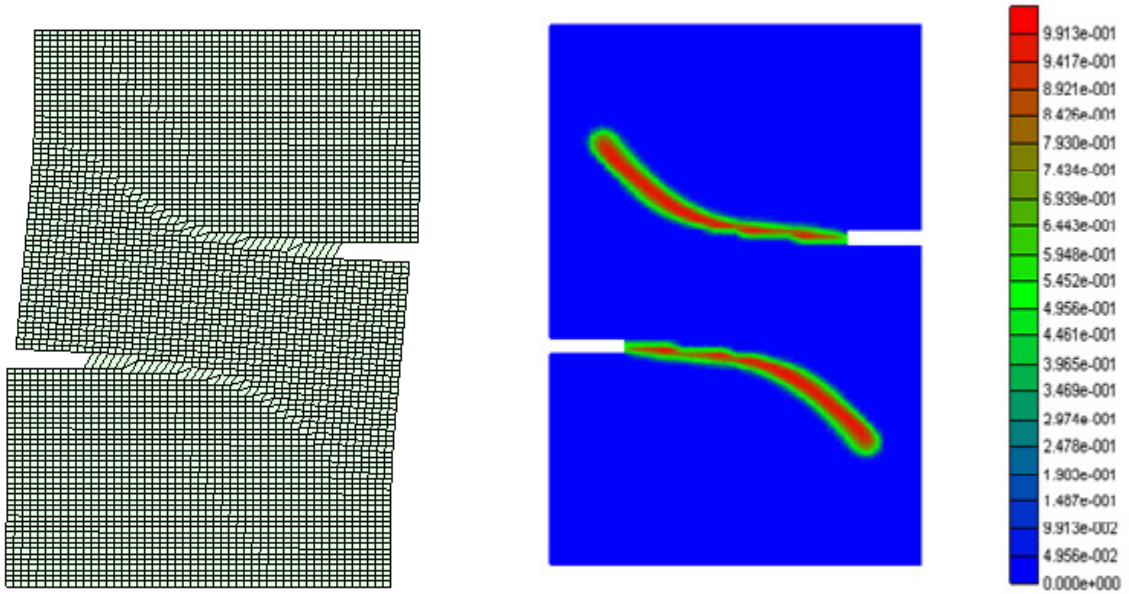

a b

Figure 34: (a) Exaggerated deformed mesh plot, (b) Damage indicator contour plot at last displacement increment.

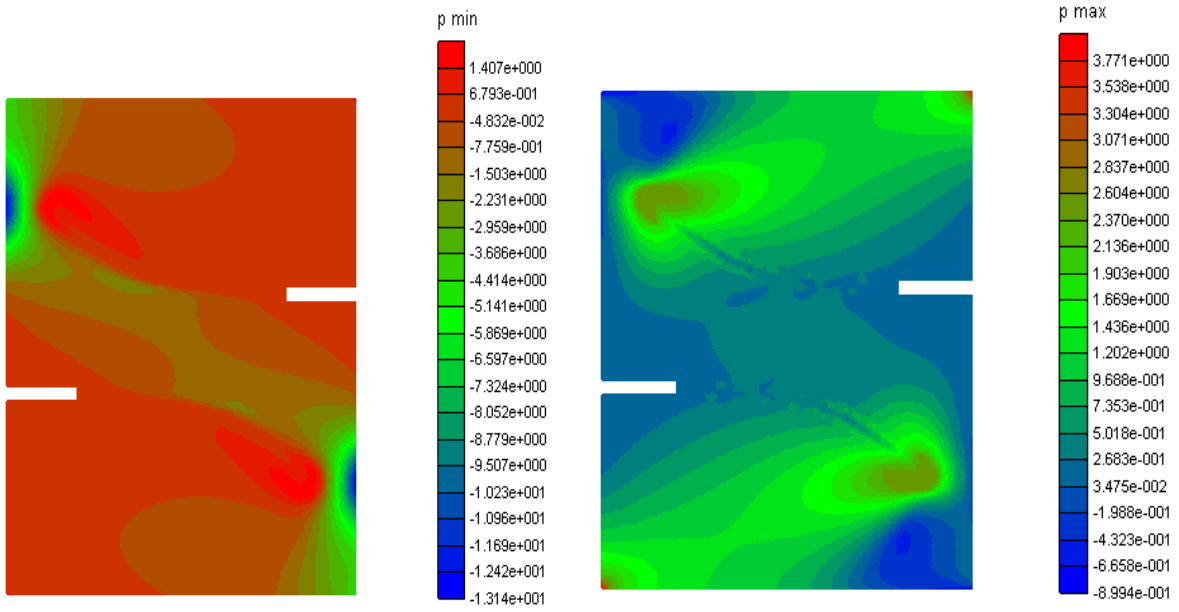

a b

Figure 35: (a) Minimum principal stress contour plot, (b) Maximum principal stress contour plot, both at final displacement step.

The results in figure 36 give a displacement verses vertical stress graph for both the 40 and 100 step solutions. The vertical stress in these plots is the sum of the vertical forces (reactions) on the upper surface divided by the un-notched cross-sectional area (i.e. the area at the top of the specimen). We note that the average vertical stress becomes compressive in the latter stages of the analysis. This is consistent with the formation of a diagonal compression zone across the centre of the specimen (see figure 35).

As with all other examples, the SUR solutions are far more efficient than the reference Secant solution, but it is also noted that in this example the predictive-SUR solution is noticeably more efficient than the standard SUR solution.

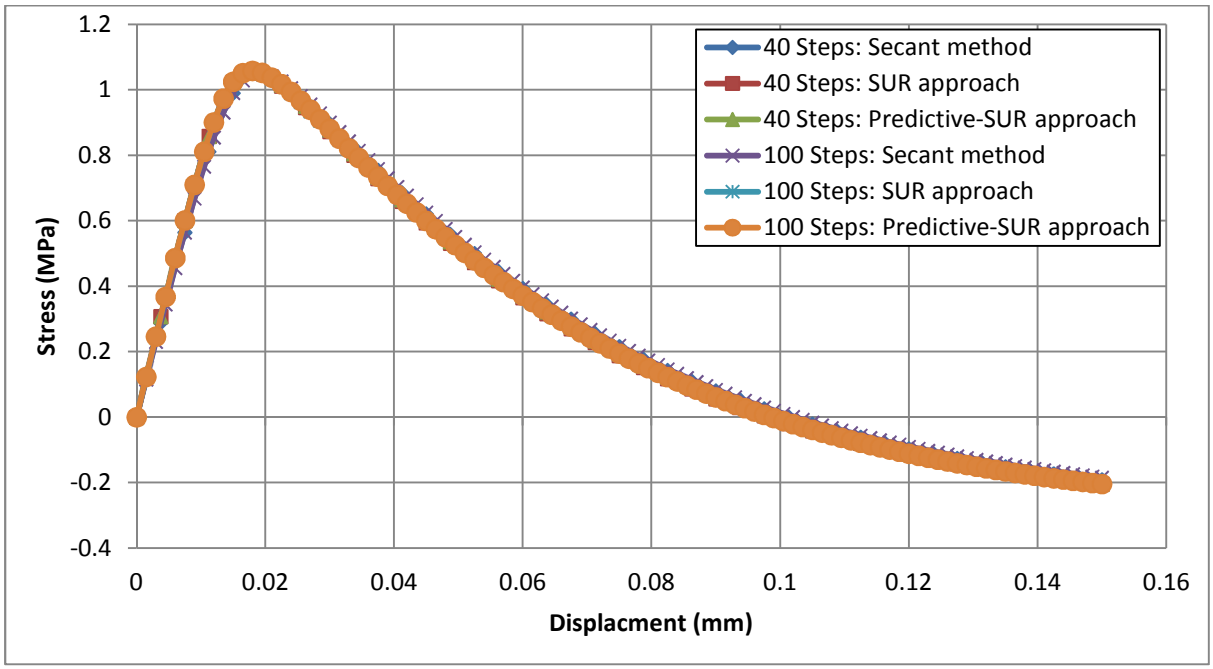

Figure 36: Numerical displacement and vertical stress responses for 40 and 100 prescribed displacement increments.

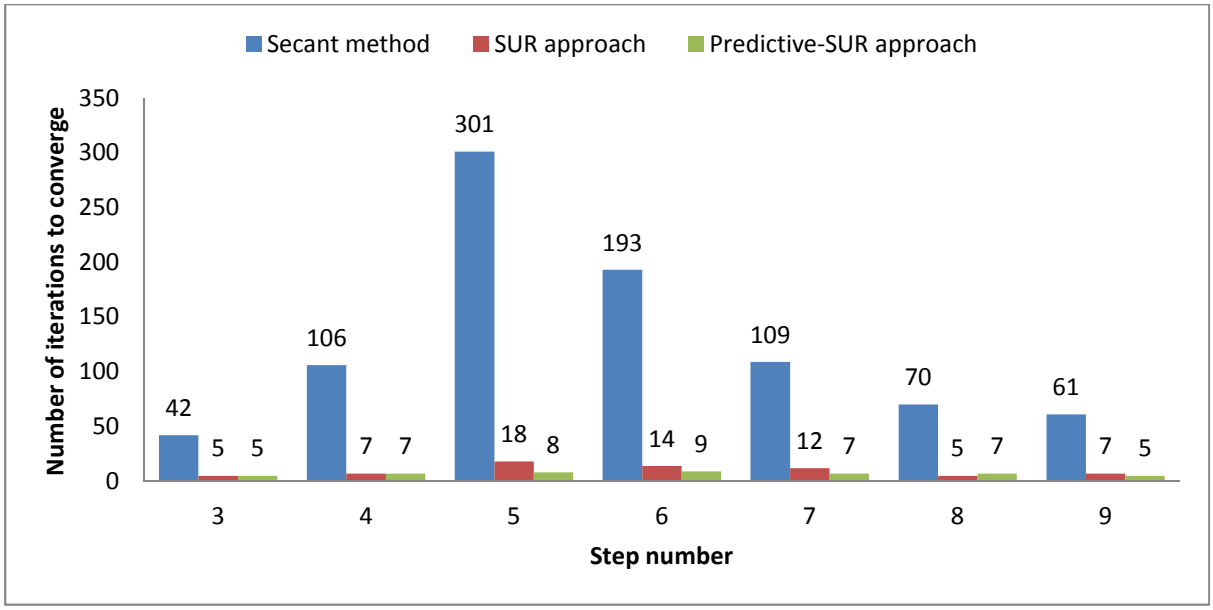

Figure 37: Number of iterations to achieve convergence for the most difficult increments (40 increments).

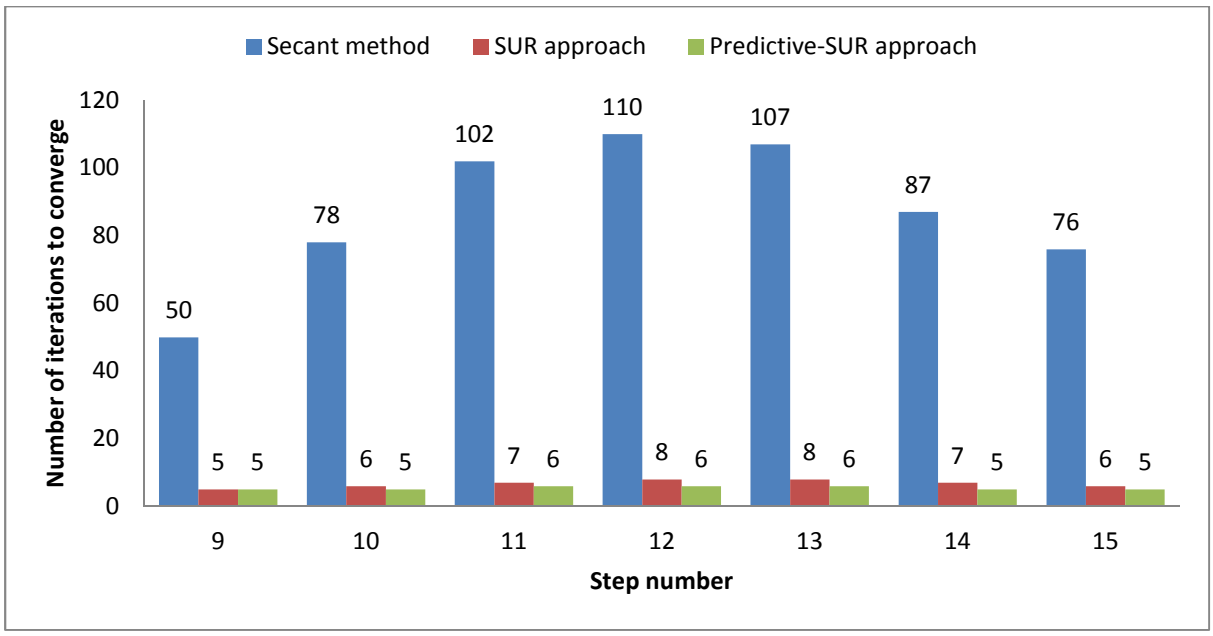

Figure 38: Number of iterations to achieve convergence for the most difficult increments (100 increments).

5.5: Two-Dimensional specimen

The purpose of this example is to illustrate the effect of varying the SUR parameters on the nonlinear solution characteristics. Therefore, unlike all of the previous examples, only the standard SUR approach is used for the analyses. The cases considered are; Case 1 [v=0.75 and a_p=0.70] and Case 2 [v=1.0 and a_p=0.8].

The analyses were carried out using a total prescribed displacement of 0.2 mm, applied over 50 steps.

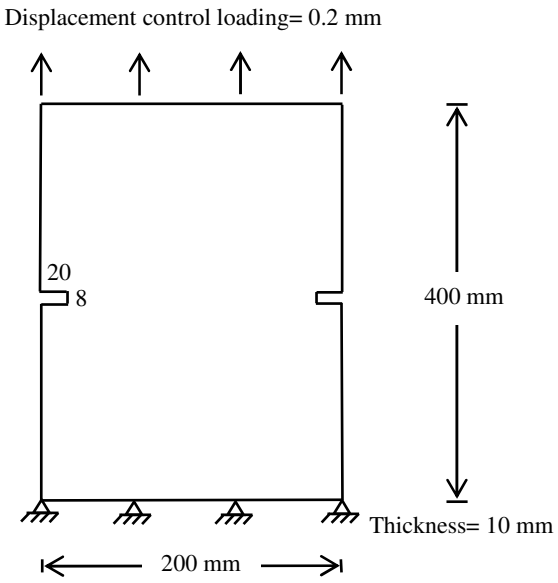

Figure 39: Dimensional details

The stress-displacement responses for both cases are given in figure 40. The iteration history in figure 41 shows that the Case 1 solution, with the standard SUR parameters, uses far fewer iterations than the Case 2 solution. The better performance of the former is attributed to the fact that the Case 1 SUR curve has a much smaller gradient at the intersection with the target curve than does the Case 2 SUR curve. This means that the 'tangent matrix' used in the Case 1 solution was closer to the true (negative) tangent and therefore resulted in less drift from the target solution in each iteration than in the Case 2 solution.

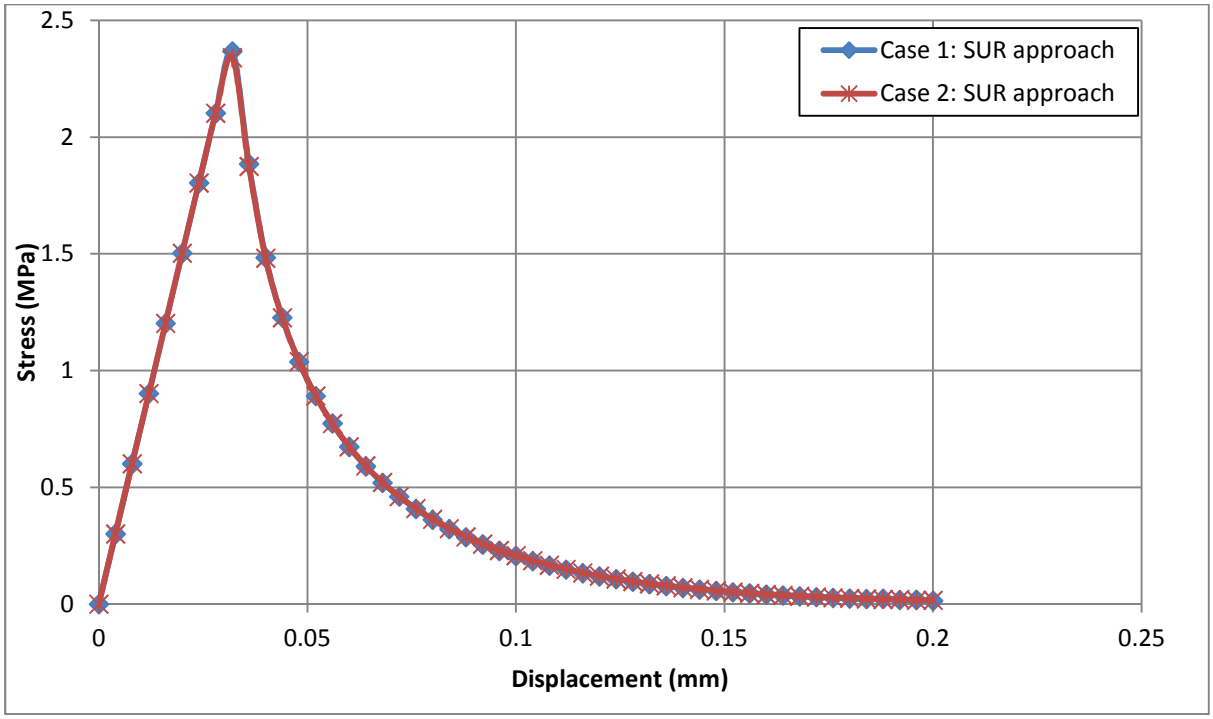

Figure 40: Displacement-Stress relationship for varying the two main parameters of SUR function.

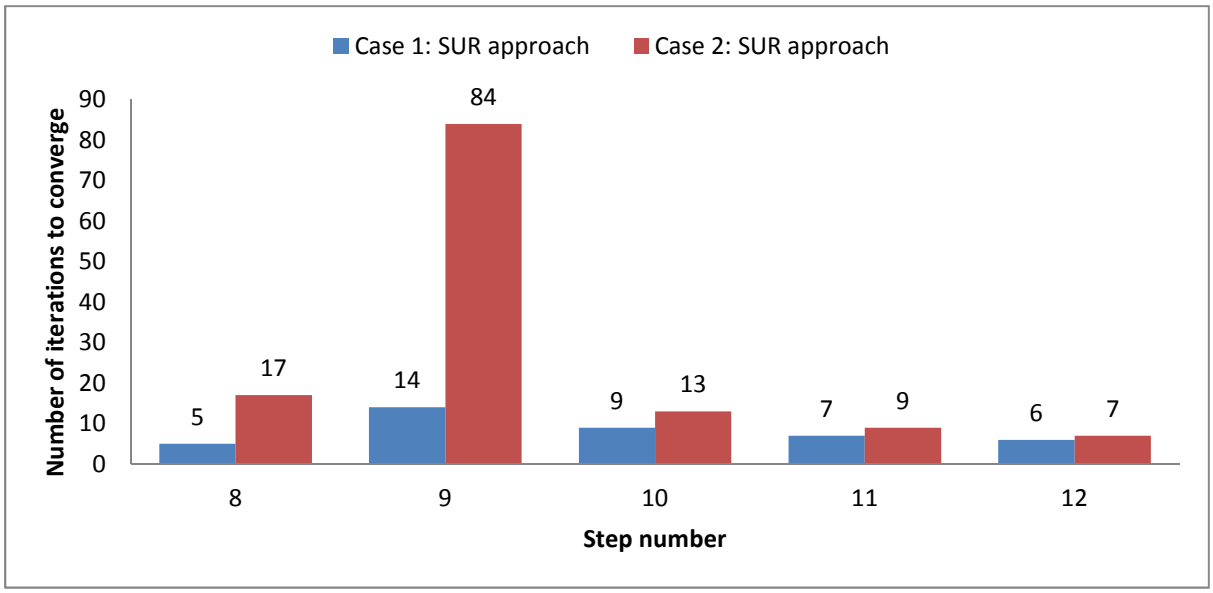

Figure 41: Number of iterations to achieve convergence for the most difficult increments for Cases 1 and 2.

6. General discussion

The conclusion from this study, and from the experience gained by using the SUR algorithm for all of the analyses presented as well as for other unreported examples, is that the suggested default parameters of 0.75 and 0.70, for v and a_p respectively, are suitable for a wide range of problems and provide the best overall balance between robustness and efficiency. These parameters may not result in the absolute minimum number of iterations in every case but they did always result in very substantial reductions in iteration numbers relative to the reference secant solutions. Overall, we found that both the standard and predictive SUR approaches were robust and never resulted in a breakdown of the nonlinear solution procedure.

In all cases, the predictive SUR algorithm resulted in fewer overall iterations than the standard SUR method. However, in the reinforced concrete example (5.3) there are particular increments for which the predictive algorithm used more iterations than the standard SUR algorithm. This is most evident in steps which follow-on from a previous step in which the predictive algorithm gave a very significant reduction in iterations (e.g. see steps 6 and 7 in Figure 31). This occurred only in the reinforced concrete example in which the cracking was more distributed than in the plain concrete examples. It is believed that temporarily freezing r_p at a predicted value causes the evolution of some local damage to be spread over 2 or 3 steps, rather over a single step. However, an important observation is that no appreciable difference in overall response, damage pattern, or stresses and strains was discernible between the two solutions (i.e. standard SUR and predictive SUR), as judged from graphs and plots of these entities.

It can be observed that examples 3 and 4 have more than one 'difficult increment' which differs from the other examples. This can be attributed to the fact that the crack pattern evolves throughout analysis and is not established in one defined step, which is in contrast to the behaviour in the other three examples.

A convergence tolerance of 0.1%, based on L2 norms of iterative displacements and out of balance forces, is sufficient for practical analyses. Using a tighter tolerance results in no appreciable change in results, as judged from damage patterns and response graphs. Using a tighter tolerance (e.g. 10^{-6}) results in more iterations than obtained with the slacker tolerance (10^{-3}), but the conclusion that the standard SUR and SUR predictive algorithms always use far fewer iterations than the reference secant solution remains unchanged.

Solutions were attempted using a standard Newton solution with a consistent tangent matrix i.e. using a form of $\mathbf{D}_{tan}$ based on the negative tangent of the target curve. We found that frequent

numerical breakdown occurred when such solutions were attempted, which is in agreement with the findings reported in much of the literature reviewed in the opening section of this paper.

7. Conclusion

The proposed model is developed to work with an incremental iterative nonlinear FE solution scheme and thus it is compatible with other FE material models developed for this standard type of solution algorithm.

The proposed SUR approach, which applies a smooth unloading-reloading function in a damage model and then uses this function as a basis for computing an approximate positive-definite finite element tangent matrix, is robust and results in considerable savings relative to a model that uses a secant unloading-reloading function. A new method for predicting the converged value of a damage evolution parameter, based on an extrapolation in semi-log space, is effective and results in significant savings in terms of the total number of iterations required for a complete solution. In all examples, the performance of this predictive-SUR approach equalled, or bettered that of, the standard SUR approach.

The form of the SUR function greatly affects the convergence characteristics of the model, with functions that have small gradients at the intersection with the target softening curve performing best.

Acknowledgements

The finite element company LUSAS (www.lusas.com) is gratefully acknowledged for their support.

References

1. van Mier, J.G.M., *Fracture Processes of Concrete*. 1996: Taylor & Francis.
2. Karihaloo, B.L., *Fracture Mechanics and Structural Concrete*. 1995: Longman Scientific & Technical.
3. Bažant, Z.P. and Planas, J., *Fracture and Size Effect in Concrete and Other Quasibrittle Materials*. 1997: Taylor & Francis.
4. van Mier, J.G.M., *Concrete Fracture: A Multiscale Approach*. 2012: Taylor & Francis.
5. De Borst, R., Crisfield, M.A., Remmers, J.J.C.and Verhoosel, C.V., *Nonlinear Finite Element Analysis of Solids and Structures*. 2012: Wiley.
6. Bažant, Z.P. and Oh, B.H., *Crack band theory for fracture of concrete.* Material and Construction, 1983. **16**(3): p. 155-177.
7. Pijaudier-Cabot, G. and Bažant, Z., *Nonlocal Damage Theory.* Journal of Engineering Mechanics, 1987. **113**(10): p. 1512-1533.
8. Jirásek, M. and Marfia, S., *Non-local damage model based on displacement averaging.* International Journal for Numerical Methods in Engineering, 2005. **63**(1): p. 77-102.
9. Ru, C.Q. and Aifantis, E.C., *A simple approach to solve boundary-value problems in gradient elasticity.* Acta Mechanica, 1993. **101**(1-4): p. 59-68.
10. Peerlings, R.H.J., deBorst, R., Brekelmans, W.A.M.and deVree, J.H.P., *Gradient enhanced damage for quasi-brittle materials.* International Journal for Numerical Methods in Engineering, 1996. **39**(19): p. 3391-3403.
11. de Borst, R., Pamin, J.and Geers, M.G.D., *On coupled gradient-dependent plasticity and damage theories with a view to localization analysis.* European Journal of Mechanics - A/Solids, 1999. **18**(6): p. 939-962.
12. Rodríguez-Ferran, A., Bennett, T., Askes, H.and Tamayo-Mas, E., *A general framework for softening regularisation based on gradient elasticity.* International Journal of Solids and Structures, 2011. **48**(9): p. 1382-1394.
13. Crisfield, M.A., *Non-linear Finite Element Analysis of Solids and Structures*. Vol. Vol.1. 1991, Chichester, UK.: John Wiley & Sons.
14. Dennis, J. J. and Moré, J., *Quasi-Newton Methods, Motivation and Theory.* SIAM Review, 1977. **19**(1): p. 46-89.
15. Crisfield, M.A., *Accelerated solution techniques and concrete cracking.* Computer Methods in Applied Mechanics and Engineering, 1982. **33**(1–3): p. 585-607.
16. Ma, S.Y.A. and May, I.M., *The Newton-Raphson method used in the non-linear analysis of concrete structures.* Computers & Structures, 1986. **24**(2): p. 177-185.
17. Crisfield, M.A., *Non-linear Finite Element Analysis of Solids and Structures*. Vol. Vol.2. 1997, Chichester, UK.: John Wiley & Sons.
18. Wempner, G.A., *Discrete approximations related to nonlinear theories of solids.* International Journal of Solids and Structures, 1971. **7**(11): p. 1581-1599.
19. Riks, E., *An incremental approach to the solution of snapping and buckling problems.* International Journal of Solids and Structures, 1979. **15**(7): p. 529-551.
20. Ramm, E., *Strategies for Tracing the Nonlinear Response Near Limit Points*, in *Nonlinear Finite Element Analysis in Structural Mechanics*, W. Wunderlich, Stein, E. and Bathe, K.J., Editors. 1981, Springer Berlin Heidelberg. p. 63-89.
21. Pohl, T., Ramm, E.and Bischoff, M., *Adaptive path following schemes for problems with softening.* Finite Elements in Analysis and Design, 2014. **86**(0): p. 12-22.
22. Ladeveze, P. and Simmonds, J.G., *Nonlinear Computational Structural Mechanics: New Approaches and Non-Incremental Methods of Calculation*. 1999: Springer New York.
23. Kerfriden, P., Allix, O.and Gosselet, P., *A three-scale domain decomposition method for the 3D analysis of debonding in laminates.* Computational Mechanics, 2009. **44**(3): p. 343-362.

24. Vandoren, B., De Proft, K., Simone, A.and Sluys, L.J., *A novel constrained LArge Time INcrement method for modelling quasi-brittle failure.* Computer Methods in Applied Mechanics and Engineering, 2013. **265**(0): p. 148-162.
25. Oliver, J., Huespe, A.E., Blanco, S.and Linero, D.L., *Stability and robustness issues in numerical modeling of material failure with the strong discontinuity approach.* Computer Methods in Applied Mechanics and Engineering, 2006. **195**(52): p. 7093-7114.
26. Oliver, J., Huespe, A.E.and Cante, J.C., *An implicit/explicit integration scheme to increase computability of non-linear material and contact/friction problems.* Computer Methods in Applied Mechanics and Engineering, 2008. **197**(21–24): p. 1865-1889.
27. Rots, J.G., *Sequentially linear continuum model for concrete fracture. In: de Borst R, Mazars J, Pijaudier-Cabot G, van Mier, JGM, Balkema AA, editors. Fracture Mechanics of concrete Structures. The Netherlands: Liss.* 2001: p. 831-839.
28. Rots, J.G. and Invernizzi, S., *Regularized sequentially linear saw-tooth softening model.* International Journal for Numerical and Analytical Methods in Geomechanics, 2004. **28**(7-8): p. 821-856.
29. Rots, J.G., Belletti, B.and Invernizzi, S., *Robust modeling of RC structures with an "event-by-event" strategy.* Engineering Fracture Mechanics, 2008. **75**(3–4): p. 590-614.
30. DeJong, M.J., Hendriks, M.A.N.and Rots, J.G., *Sequentially linear analysis of fracture under non-proportional loading.* Engineering Fracture Mechanics, 2008. **75**(18): p. 5042-5056.
31. Graça-e-Costa, R., Alfaiate, J., Dias-da-Costa, D., Neto, P.and Sluys, L.J., *Generalisation of non-iterative methods for the modelling of structures under non-proportional loading.* International Journal of Fracture, 2013. **182**(1): p. 21-38.
32. Slobbe, A.T., Hendriks, M.A.N.and Rots, J.G., *Sequentially linear analysis of shear critical reinforced concrete beams without shear reinforcement.* Finite Elements in Analysis and Design, 2012. **50**(0): p. 108-124.
33. Oliver, J., Cervera, M., Oller, S.and Lublineer, J., *Isotropic Damage Models and Smeared Crack Analysis of Concrete.* Computer Aided Analysis and design of Concrete Structures, Proceedings of SCI-C 1990, II. International Conference, Austria, 1990: p. 945-957.
34. Oliver, J., Huespe, A.E., Pulido, M.D.G.and Chaves, E., *From continuum mechanics to fracture mechanics: the strong discontinuity approach.* Engineering Fracture Mechanics, 2002. **69**(2): p. 113-136.
35. Jirásek, M., *Damage and Smeared Crack Models*, in *Numerical Modeling of Concrete Cracking*, G. Hofstetter and Meschke, G., Editors. 2011, Springer Vienna. p. 1-49.
36. Reinhardt, H.W., *Fracture mechanics of an elastic softening material like concrete*. 1984, Delft, Netherlands: Stevin-Laboratory of the Dept. of Civil Engineering, Delft University of Technology.
37. Elfgren, L. and Noghabai, K., *Tension of reinforced concrete prisms. Round robin analysis and tests on bond: .* a report from an investigation arranged by RILEM Technical Committee 147-FMB Fracture Mechanics to Anchorage and Bond Research Report. Luleå University of Technology, Division of Structural Engineering, 2001.

Appendix

Appendix A: Target softening function

It is recalled that the target softening function, neglecting the initial linear part of equation (5), is given by:

$$f_s(r_p) = \frac{a_t \cdot f_t}{\beta - 1} \cdot e^{-c_1 \cdot \eta} \cdot (\beta - e^{-c_1 \cdot m \cdot \eta}) \quad \text{(A1)}$$

Constants m, β, and a_t are computed such that the function satisfies the following conditions:

$$f_s = a_t f_t \quad at \quad \eta = 0 \quad \text{(A2a)}$$

$$\frac{\partial f_s}{\partial r_p} = E \quad at \quad \eta = 0 \quad \text{(A2b)}$$

$$f_s = f_t \quad at \quad \eta = \eta_k \quad \text{(A2c)}$$

$$\frac{\partial f_s}{\partial \eta} = 0 \quad at \quad \eta = \eta_k \quad \text{(A2d)}$$

Noting that $a_t f_t$ denotes the end of the linear portion of the stress-strain curve and that $a_t \in [0, 1]$. Equation (A2a) is automatically satisfied by the function form given in (A1).

Differentiating equation (A1), and applying the condition (A2b) in the resulting expression, leads to:

$$\beta = \frac{r_\varepsilon + a_t c_1 (1 + m)}{r_\varepsilon + a_t c_1} \quad \text{(A3)}$$

in which $r_\varepsilon = \frac{r_0}{r_t}$

Applying condition (A2c) and using equation (A3) leads to:

$$a_t = \frac{m \cdot \left(e^{c_1 \eta_k} + \frac{r_\varepsilon}{c_1} \right)}{1 + m - e^{c_1 m \eta_k}} - \frac{r_\varepsilon}{c_1} \quad \text{(A4)}$$

Condition (A2d) may be used to derive the following equation:

$$\eta_k = \frac{- ln\left(\frac{r_\varepsilon + a_t c_1 (m+1)}{(m+1)(r_\varepsilon + a_t c_1)} \right)}{c_1 m} \quad \text{(A5)}$$

η_k may also be expressed as:

$$\eta_k = \frac{a_k - a_t}{r_\varepsilon} \tag{A6}$$

The SUR function (equation 6) should pass through the peak point of the target curve. This condition is used to choose the value of a_k. If r_{eff} is set to r_p in (equation 6), f_s is set to f_t and σ_k to $a_k f_t$, then a_k is given by:

$$a_k = \frac{1}{v \cdot \left[1 - (1 - \frac{a_p}{v}) \cdot e^{-\left[\frac{1-a_p}{v-a_p}\right]} \right]} \tag{A7}$$

It is recalled that a_p is set to 0.70 and v set to 0.75.

(A4) and (A6) are used to find m and a_t respectively, but it is noted that these values vary with r_ε and thus with r_0. The numerical solution (using a Mathcad program) to equation (A4) to (A6) was used to derive the following approximate function form, which provides a close fit to the true value of m for a wide range of r_ε. The maximum error in m is under 7% for a range of r_ε from 20 to 600 and such a difference in m produce a negligible change in the f_s function <0.1%.

$$m_{approximate} = 0.805 \cdot r_\varepsilon^{1.392} \tag{A8}$$

The numerical solution for m also determined associated values of a_t but, rather than also creating an approximate function for a_t, it was found more convenient to use equation (A8) to compute m and then an initial value of $a_t = a_p$ is used to compute η_k, after which this value is used in repeated direct substitutions of η_k in equation (A4) to find a_t. It should be mentioned that 3 iterations gives < 0.1% error.